CHEMISTRY OF BRINE IN AN UNCONVENTIONAL SHALE DOMINATED SOURCE BED UNDERSTANDING WATER- ORGANIC MATERIAL-MINERAL INTERACTIONS DURING HYDROCARBON GENERATION

by

HELDER IVAN ALVAREZ

B.S., Kansas State University, 2013

A THESIS

submitted in partial fulfillment of the requirements for the degree

MASTER OF SCIENCE

Department of Geology
College of Arts and Sciences

KANSAS STATE UNIVERSITY
Manhattan, Kansas

2015

Approved by:

Major Professor
Dr. Sambhudas Chaudhuri

Copyright

Abstract

The exploration and development of unconventional shale plays provide an opportunity to study the hydrocarbon generation process. These unconventional plays allow one to investigate the interactions between the fluid, mineral, and organic material that occur in a hydrocarbon-generating source bed, before any changes in composition that may occur during secondary migration or post migration processes. Previous studies have determined the chemical constituents of formation waters collected from conventional reservoirs after secondary migration has occurred. This investigation targets formation waters collected from the Woodford shale that acts as both source and reservoir, therefore samples have yet to experience any changes in composition that occur during secondary migration. This investigation focuses on the major element and trace element chemistry of the formation water (Cl, Br, Na, K, Rb, Mg, Ca, Sr, and Rare Earth Elements), which has been compared to chemical constituents of the associated crude oil and kerogens. Analytical data for this investigation were determined by the following methods; Ion Chromatography, Inductively Coupled Plasma Mass Spectrometry (ICP-MS), and Inductively Coupled Plasma Atomic Emission Spectroscopy (ICP-AES). The information is used to assess the presence of different sources of water that constitute the formation water, and also to investigate interaction between different minerals and formation waters within the source beds. The formation water data also yields new insights into compartmentalization of oil-gas rich zones within the source beds.

Table of Contents

List of Figures

List of Tables

Acknowledgements

I would first like to thank my Graduate Advisors, Dr. Sambhudas Chaudhuri and Dr. Matthew Totten, for their guidance and support during my time at Kansas State University. I would like to thank Greg Riepl, John Miesse, and Steve Kirkwood for their support as alumni, with your support I was able to carry out my research. Thank you Magdaleno Alvarez and Marisa Alvarez for being the greatest parents I could have ever dreamed of, your love, support, and guidance has molded me into the person I am today. I also want to extend a thank you to my entire family your love and support does not go unnoticed. Finally thank you to all the wonderful people I have had the privilege of calling a friend.

Chapter 1 - Introduction

Hydrocarbon generation in source beds is a complex process. This process involves interactions among various types of organic matter with mineral matrices, gases, and water under the subjugation of geothermal energy associated with burial and to some extent radiation energy. Understanding the extent of interactions among these different components is necessary to correctly predict the paths of hydrocarbon generation, which has been suggested by the Chaudhuri Totten Clauer (CTC) model. Records of these interactions may be retrieved, at least partially, by analyzing kerogens, crude oil, mineral constituents, and waters. An integration of the chemical signatures of these components may go a long way towards the reconstruction of interaction pathways, and possibly even time and duration of said interactions during the hydrocarbon generation process in the source beds.

This investigation has investigated the potential chemical pathways that can describe the interactions among the kerogen, hydrocarbons, minerals, and water during hydrocarbon generation. The primary focus of this investigation is the inorganic constituents of the formation water and crude oils found in a shale source bed. Focusing on the inorganic components, an attempt on delineating the distributions of metals between crude oil and formation waters has been made. The analyses of metals in crude oil and formation waters have a long history (Witherspoon and Nagashima, 1957; Bonham, 1956; Ball et al., 1960; Hodgson, 1954; Yen, 1975). The metals that have received the most attention are vanadium and nickel, largely because their geochemical signatures in crude oil are not destroyed by migration or secondary alteration such as water washing bacterial degradation (Lewan, 1982). There are other metals which have the potential to identify source bed variations, without being impacted by migration

history. Rare earth elements (REE) and elemental ratios such as potassium and rubidium have proven to be useful indicators. The focal point of this study is on the major and trace element chemistry of the crude oil and formation water, along with the associated mineral data from Alkhammali (2015). Integration of REE and potassium-rubidium ratios data reveals information of interaction between crude oil and formation waters during hydrocarbon generation.

Trace and major element analysis of formation water date back to Collins, (1975). Available data on formation waters is essentially on waters collected from secondary reservoirs. The history of these formation waters associated with the secondary reservoir rocks is inherently complex, furthermore there are few studies focused on finding the relationship of trace metals in formation waters and crude oils in the secondary reservoirs. A deep connection exists in the evolution between formation water and crude oil, which can be established only when the two are found together in a source bed. This is the first attempt to examine what that chemical relationship could be that can shed light on the role water in crude oil generation.

The majority sampled wells for this study area are located in Payne County of north central Oklahoma, with the exception of one sample location situated south of Payne County. The crude oil and formation water samples have been collected from producing wells in the Woodford shale. The Woodford shale is an unconventional target which is drilled horizontally and completed using hydraulic fracturing techniques. The introduction of chemical additives to the fracturing fluid required a six month production history before sample collection to reduce the risk of our samples containing these additives.

Chapter 2 - Materials and Methods

The study area focuses on the Woodford shale in Payne County, Oklahoma. The samples were collected from horizontally drilled wells targeting the Woodford Shale. Crude oil, brine, and drill cutting samples were collected from various well sites in Payne County with one exception, a well in Pottawatomie County located just south of Payne County. The first samples collected were the drill cuttings, collected across known intervals, washed and packaged. Because the completion of these wells required hydraulic fracturing, collection of the crude oil and brine samples had to be delayed until after six months of initial production to mitigate the influence of chemical additives. The process of collecting the crude oil and brine samples consisted of collecting the fluids from the wellheads in thoroughly cleaned 1000ml narrow mouth Nalgene bottles, individual sealing and labeling of the sample, and packaging and transport to Kansas State University.

Preparation of Crude Oil Samples

The processing of the crude oil took place in the Chemistry and Biochemistry Department at Kansas State University closely following the methods described in Ramirez-Caro (2013). Preparation of the samples required multiple steps in order to be ready for analysis by ICP-MS. The first step required crude oil to be centrifuged to separate any additional brine that did not separate naturally. After centrifugation, 1000ml of the separated crude oil was placed in a fused silica beaker. The beaker was placed on a hot plate at 200 degrees Celsius, and

incrementally raised to 550 degrees in order to evaporate the lighter fractions of the crude oil. Once the evaporation process was completed, double vacuum distilled concentrated HNO_3 was added, then allowed to evaporate to dryness. This step was repeated with known amounts and concentrations of HNO_3 until the final solution was obtained. The last step was to filter the final solution, collect the solution in 30ml sample bottles, which then contained what will be the materials for the chemical analysis.

Analysis of Crude Oil Samples

The crude oil samples were sent to Laboratoire d'Hydrologi et da Geochimie de Strasbourg at the University of Strasbourg, France. Analytical examination was conducted by inductively coupled plasma mass spectrometry (ICP-MS), and inductively coupled plasma atomic emission spectroscopy (ICP-AES). The raw analytical data provided by Strasbourg were corrected by the amount of initial oil ashed and the amount of final solution.

Preparation and Analysis of Formation Water Samples

Preparation of the formation water involved filtering the raw formation water to remove any suspended residue in the water. The filtered water was then passed through a cation exchange chromatograph column to concentrate the REE. After the solution was processed through the columns, the samples were evaporated to dryness. The evaporated samples were dissolved in 1N highly purified HNO_3 for analysis. Processed samples were analyzed for their trace metal contents and all major element contents, except Cl, at the Laboratoire d'Hydrologi et da Geochimie de Strasbourg at the University of Strasbourg, France. Analytical examination at the University of Strasbourg was conducted by inductively coupled plasma mass spectrometry

(ICP-MS), and inductively coupled plasma atomic emission spectroscopy (ICP-AES). Cl was analyzed at Kansas State University, using an Ion Chromatograph.

Chapter 3 - Results

Crude Oil Analytical Data

Analytical results for the Woodford shale crude oil samples from Payne County, Oklahoma are shown in Table 3.1. The table illustrates the raw ICP-MS and ICP-AES data, which were ultimately correct to account for the original sample amount and the final solution amount. Elements Si to P are displayed in parts per million (ppm) and elements La to U are displayed in parts per billion (ppb). Any element concentration below detection limits are highlighted in orange. Elemental ratios were also calculated for U/Th, V/Ni, and K/Rb for each sample if possible. Figure 3.1 represents the total amount of REE in each of the samples, which range from 0.162-0.441 µg/ml of oil. Total blank correction is less than 0.1 nanogram.

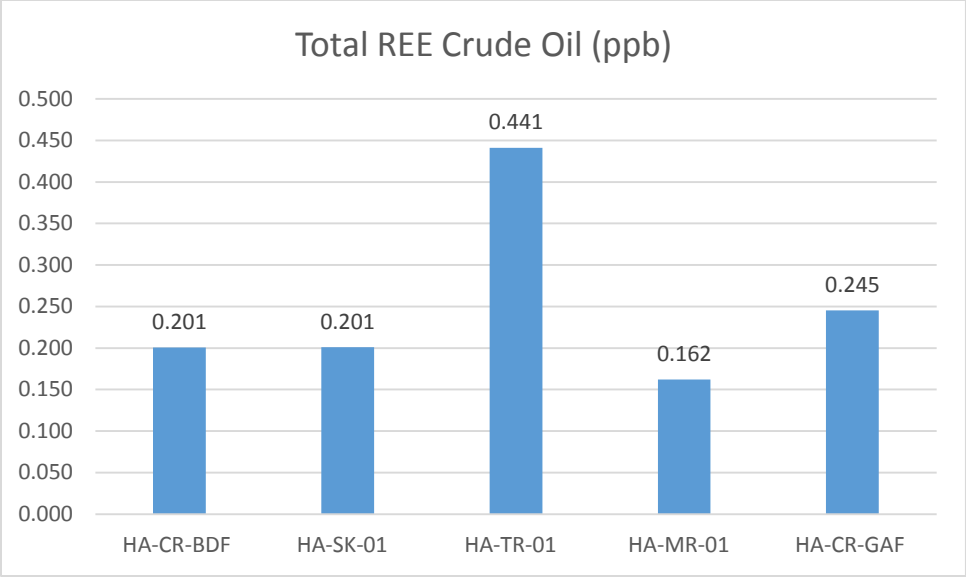

Figure 3.1 Distribution of total REE concentration in formation water samples.

	HA-CR-BDF	HA-SK-01	HA-TR-01	HA-MR-01	HA-CR-GAF
élément					
Si	0.05	0.08	0.10	0.07	0.06
Al	0.192	0.046	0.102	0.022	0.229
Mg	0.186	0.022	0.028	0.015	0.041
Ca	0.80	0.24	0.45	0.14	0.58
Fe	0.266	0.22	0.52	0.22	0.143
Mn	0.0054	0.004	0.004	0.002	0.0034
Ti	-	-	-	-	-
Na	4.26	0.56	0.33	0.27	1.83
K	0.1	-	0.07	0.07	-
P	0.023	0.15	0.32	0.09	0.035
La	0.035	0.062	0.151	0.070	0.043
Ce	0.115	0.0712	0.137	0.0463	0.125
Pr	0.0054	0.0070	0.0161	0.0047	0.0084
Nd	0.0249	0.0297	0.0675	0.0189	0.0367
Sm	0.0050	0.0078	0.0160	0.0051	0.0080
Eu	0.0009	0.0025	0.0033	0.0014	0.0011
Gd	0.0055	0.005	0.011	0.004	0.0066
Tb	0.0005	0.0008	0.0016	0.0005	0.0010
Dy	0.0032	0.0042	0.0086	0.0029	0.0058
Ho	0.0007	0.0018	0.0169	0.0004	0.0014
Er	0.0022	0.0020	0.0039	0.0015	0.0034
Tm	0.0006	0.0002	0.0006	0.0003	0.0004
Yb	0.0012	0.0065	0.0072	0.0055	0.0037
Lu	0.0006	0.0004	0.0005	0.0007	0.0009
Cr	51	10.3	12.6	10.2	15
Co	2	20	92	34	2
Ni	34	9021	47400	15800	669
Cu	20	4.1	6.3	4.1	43
Zn	20	111	606	200	43
Rb	0.087	0.072	0.146	0.106	0.086
Sr	70.9	15	3	4	10.4
Y	0.0352	0.04	0.06	0.05	0.0332
Zr	-	0.22	0.22	0.39	-
Cd	0.079				0.063
Cs	0.008	-	-	-	0.008
Ba	61.6	1.3	2.4	1.1	12.1
V	03.0	21000	30500	25800	1880.0
Pb	2.88	1.16	1.73	1.43	1.72
Th	-	0.009	0.009	0.016	-
U	0.0095	0.0069	0.0113	0.0073	0.0177
U/Th	-	0.766666667	1.255555556	0.45625	-
V/Ni	0.08823529	2.327901563	0.643459916	1.632911392	2.810164425
K/Rb	1149.42529	-	479.4520548	660.3773585	-
ΣREE	0.201	0.201	0.441	0.162	0.245

Table 3.1 Major and trace element analytical results for Woodford shale crude oil

Crude Oil REE Distribution Patterns

The RRE distribution patterns for the crude oil samples are shown in Figures3.2-3.6. The raw ICP-MS data was corrected to account for initial sample and final solution amounts and normalized to the Post Archean Australian Shale (PAAS). The crude oil rare earth element distribution curves vary from one another.

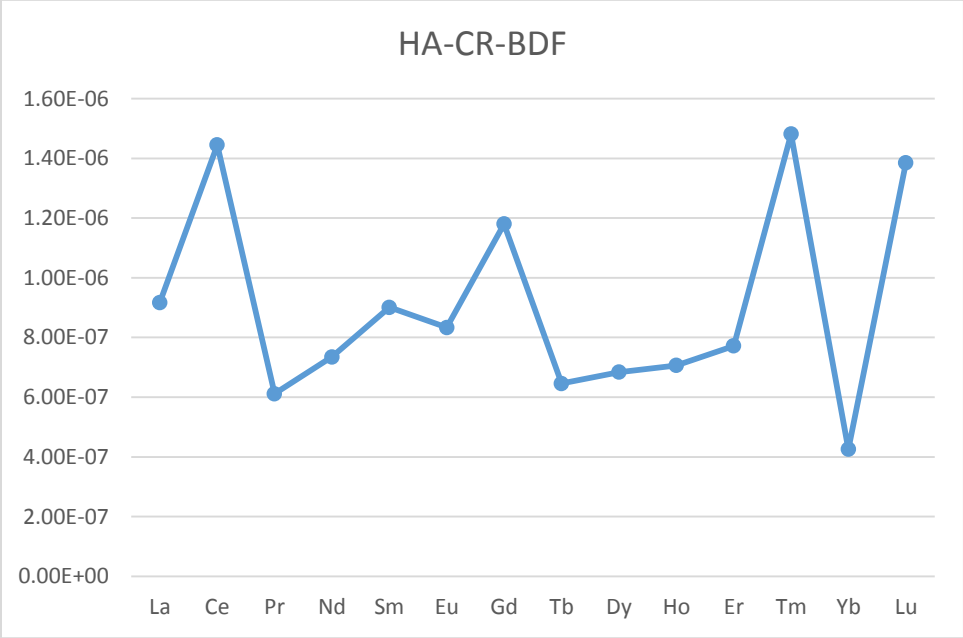

Figure 3.2 Relative distribution pattern of REE concentrations in crude oil sample (HA-CR-BDF) normalized to PAAS

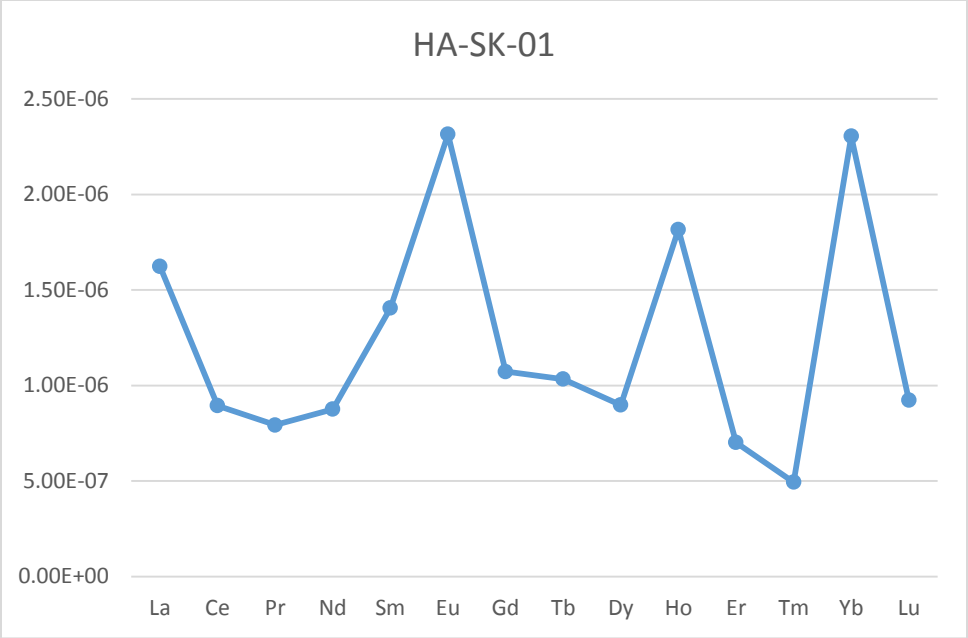

Figure 3.3 Relative distribution pattern of REE concentrations in crude oil sample (HA-SK-01) normalized to PAAS

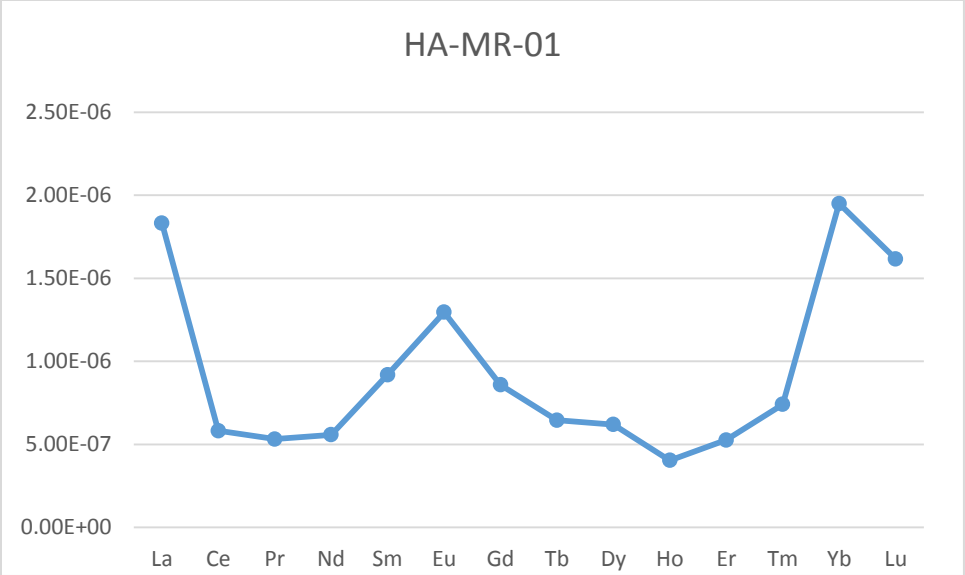

Figure 3.4 Relative distribution pattern of REE concentrations in crude oil sample (HA-MR-01) normalized to PAAS

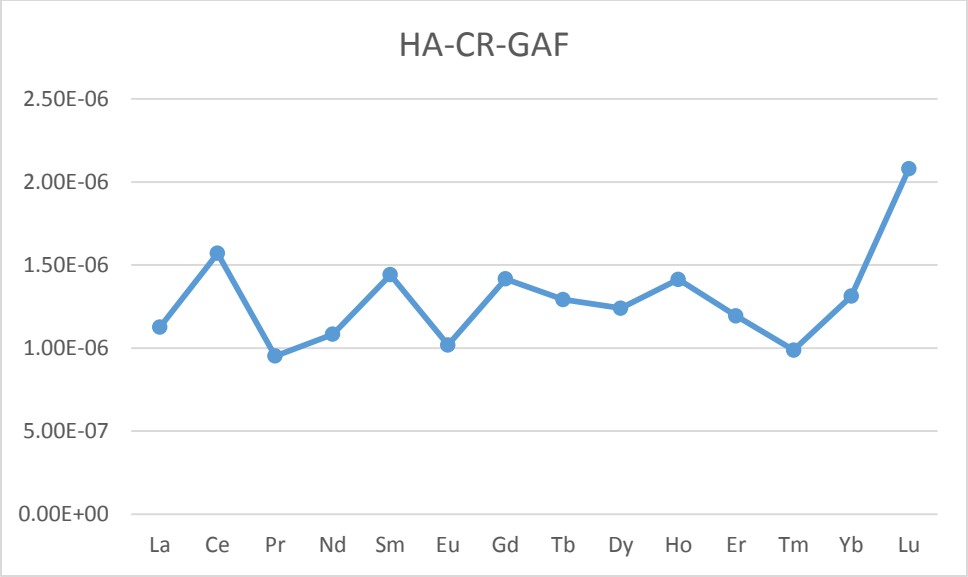

Figure 3.5 Relative distribution pattern of REE concentrations in crude oil sample (HA-CR-GAF) normalized to PAAS

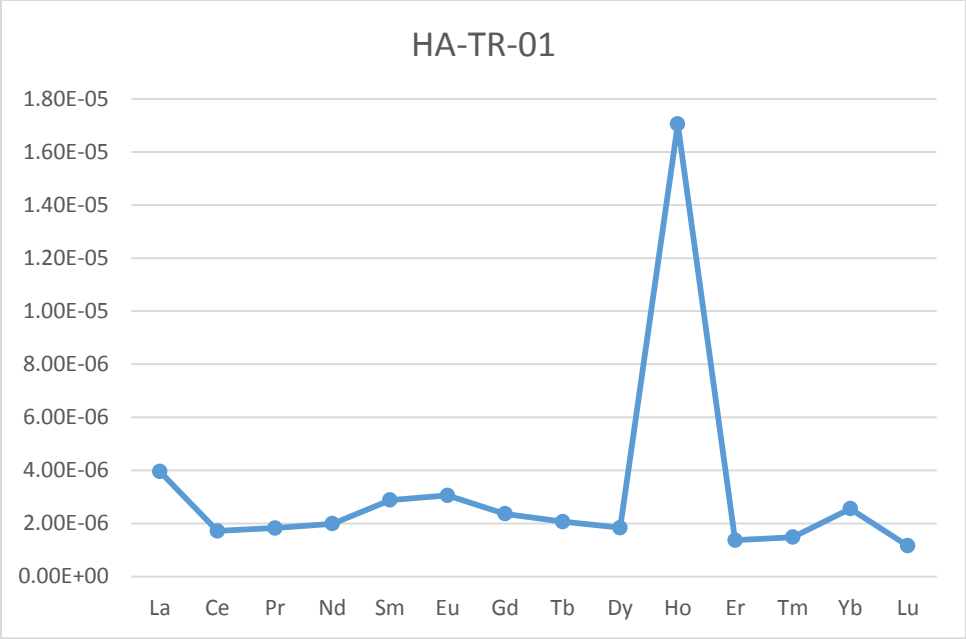

Figure 3.6 Relative distribution pattern of REE concentrations in crude oil sample (HA-TR-01) normalized to PAAS

K/Rb Ratios of Crude Oil Samples

K/Rb ratios of the crude oil samples have been calculated and plotted in figure 3.7. The K/Rb ratios of the crude oil have been compared to the K/Rb ratio of average silicate minerals from (Chaudhuri 2007). Ratios of the crude oil samples range from 660-1730 which is well above the average silicate minerals ratios. These ratios are indicative of organic influence.

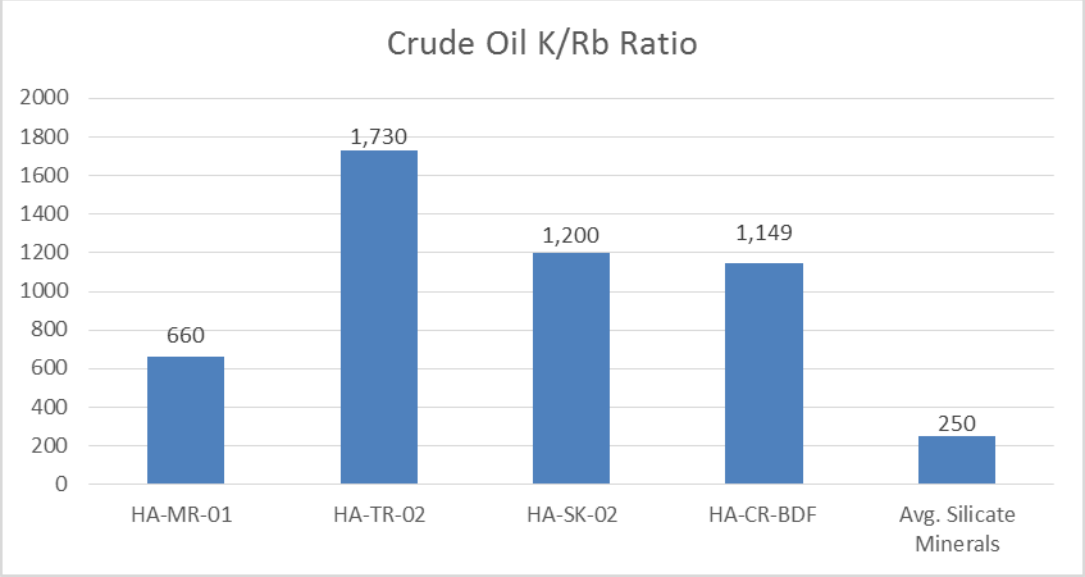

Figure 3.7 K/Rb ratios of crude oil samples (HA-MR-01, HA-TR-01, HA-SK-01, HA-CR-BDF). Average of silicate minerals included for reference (Chaudhuri et al., 2007).

Results of Formation Water

Analytical data for the Woodford shale formation samples are shown below in Table 3.2. The table illustrates the raw ICP-MS, ICP-AES, and Ion Chromatography data. The data was corrected to account for the original sample amount and the final solution amount. Elements Si to P are displayed in parts per million (ppm) and elements Cr to U are displayed in parts per billion (ppb). Any element concentration below detection limits have been highlighted in orange

for each sample. If possible elemental ratios were also calculated for U/Th, V/Ni, and K/Rb along with total rare earth elements for each sample.

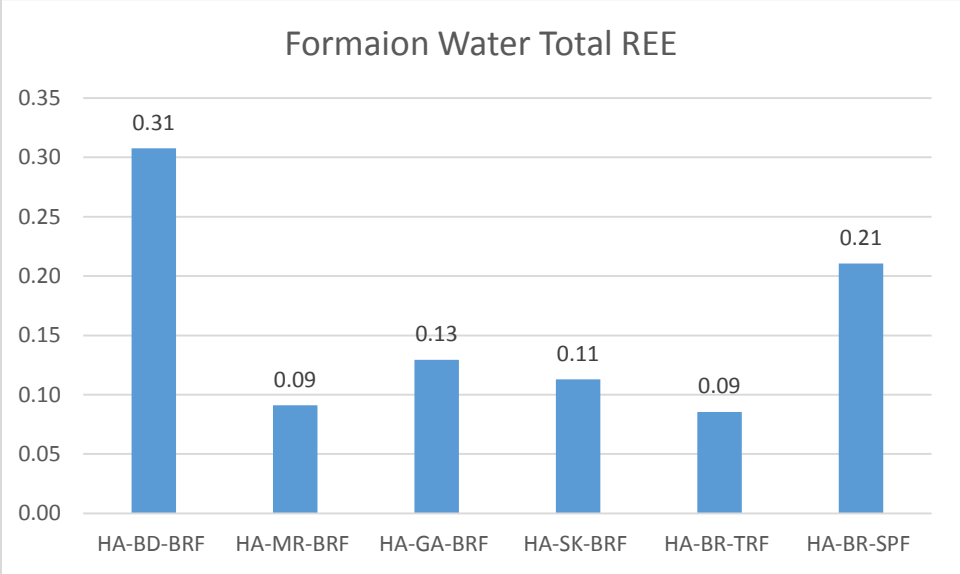

Figure 3.8 Distribution of total REE concentration in formation water samples.

REE Distribution Patterns of Formation Water Samples

The distribution curves of the REEs in the formation water samples are represented in the Figures 3.9 to 3.14. The formation water raw ICP-MS data was corrected to account for initial sample and final solution amounts. With the data corrected each sample was then normalized to the Post Archean Australian Shale (PAAS). The formation water distribution curves are similar with very little variation from one another.

élément	HA-BD-BRF	HA-MR-BRF	HA-GA-BRF	HA-SK-BRF	HA-BR-TRF	HA-BR-SPF
La	0.078	0.04833	0.06126	0.05835	0.04125	0.10179
Ce	0.10545	0.009	0.01872	0.01338	0.01428	0.01461
Pr	0.012762	0.000849	0.001995	0.001407	0.001413	0.000888
Nd	0.0594	0.012966	0.019986	0.015648	0.011451	0.027408
Sm	0.020301	0.007569	0.010284	0.009201	0.006129	0.0321
Eu	-	-	-	-	-	-
Gd	0.02265	0.009678	0.01365	0.012069	0.007923	0.028248
Tb	0.001218	0.000039	0.000138	0.000093	0.000216	0.000087
Dy	0.00453	0.000411	0.000672	0.000537	0.001149	0.000846
Ho	0.000693	0.000081	0.000132	0.000132	0.000165	0.000249
Er	0.001371	0.000195	0.000339	0.0003	0.000438	0.000504
Tm	0.000159	0.000114	0.000156	0.000114	0.000087	0.000297
Yb	0.000861	0.001368	0.001428	0.001197	0.000681	0.00228
Lu	0.000375	0.000594	0.000615	0.000519	0.000231	0.001227
Th	0.088	-	0.05	0.07	-	-
U	0.0095	0.0100	0.0103	0.0098	0.0283	0.0072
V	2	1	1	2	-	-
Ni	14	18	6	61	3.0000	3.0000
V/Ni	0.142857143	0.055555556	0.166666667	0.032786885	-	-
U/Th	0.107954545	-	0.206	0.14	-	-
ΣREE	0.31	0.09	0.13	0.11	0.09	0.21

élément	HA-TR-BR	HA-SK-BR	HA-BD-BR	HA-MR-BR	HA-GA-BR
Si	4.8	2.0	6.6	3.6	2.8
Al	0.06	0.06	0.14	0.08	0.06
Mg	1600	1840	2160	1830	1650
Ca	6520	8860	10100	8680	8700
Fe	0.08	1.00	13.4	0.34	0.86
Mn	0.728	1.85	1.57	1.23	2.06
Ti	0.80	0.76	0.74	0.78	0.78
K	403	304	655	325	276
P	1.84	0.62	0.16	0.96	1.44
Cr	12	12	10	-	-
Co	19.0	23.8	28.0	24.2	24.8
Ni	146	204	256	179	194
Cu	9.8	13.6	25.0	12.4	13.6
Zn	74.8	115	2560	76.0	286
Rb	672	610	1280	658	634
Sr	446000	640000	566000	646000	674000
Y	2.90	5.48	4.51	5.31	6.04
Zr	-	-	0.8	-	-
Cd	0.060	0.074	0.206	0.058	0.182
Cs	48.5	40.4	111	45.1	43.7

Table 3.2 Major and trace element analytical results for Woodford shale formation water

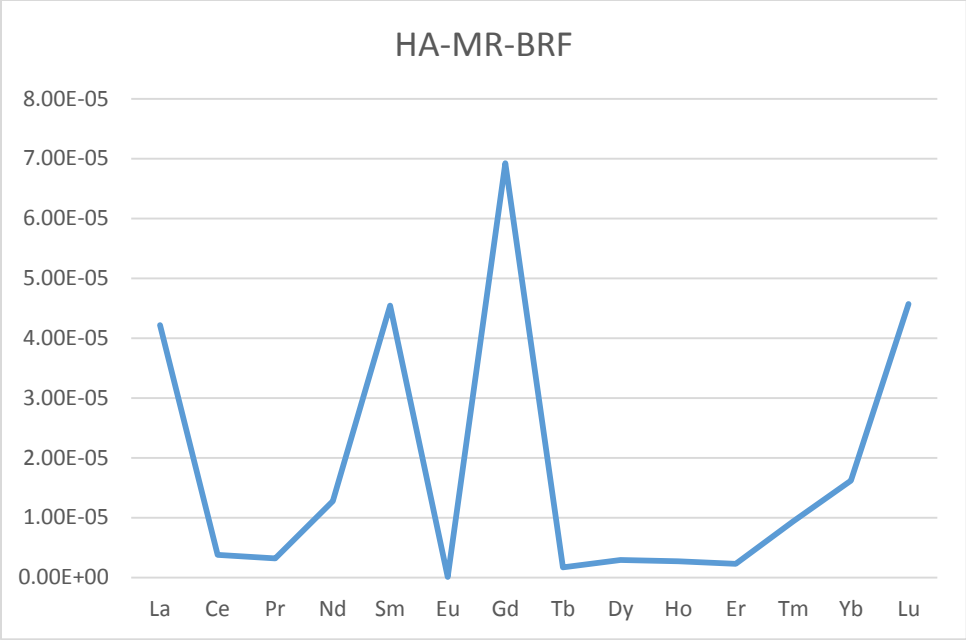

Figure 3.9 Relative distribution pattern of REE concentrations in formation water sample (HA-MR-BRF) normalized to PAAS

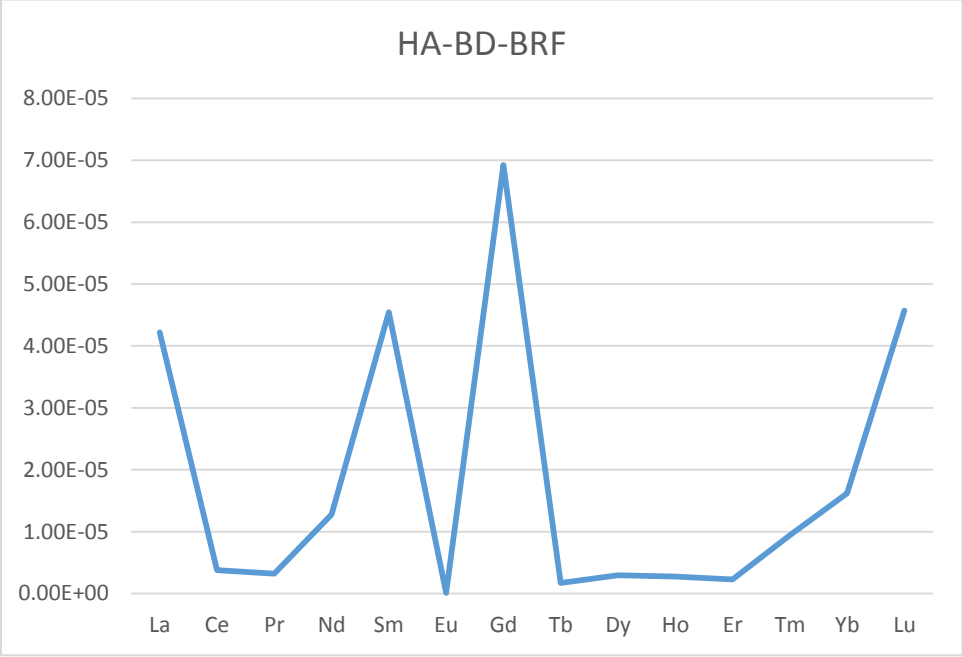

Figure 3.10 Relative distribution pattern of REE concentrations in formation water sample (HA-BD-BRF) normalized to PAAS

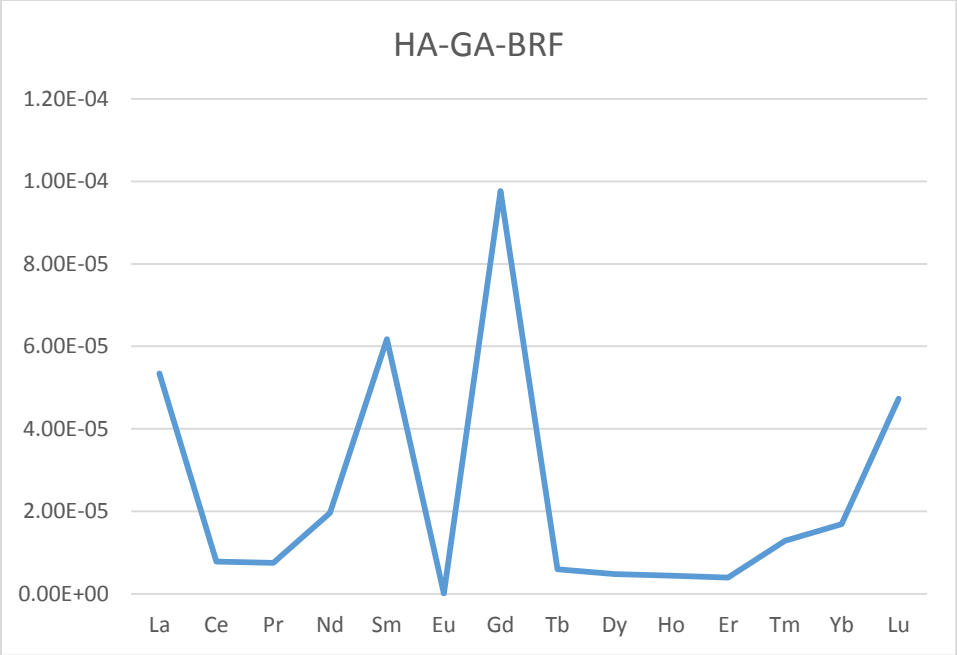

Figure 3.11 Relative distribution pattern of REE concentrations in formation water sample (HA-GA-BRF) normalized to PAAS

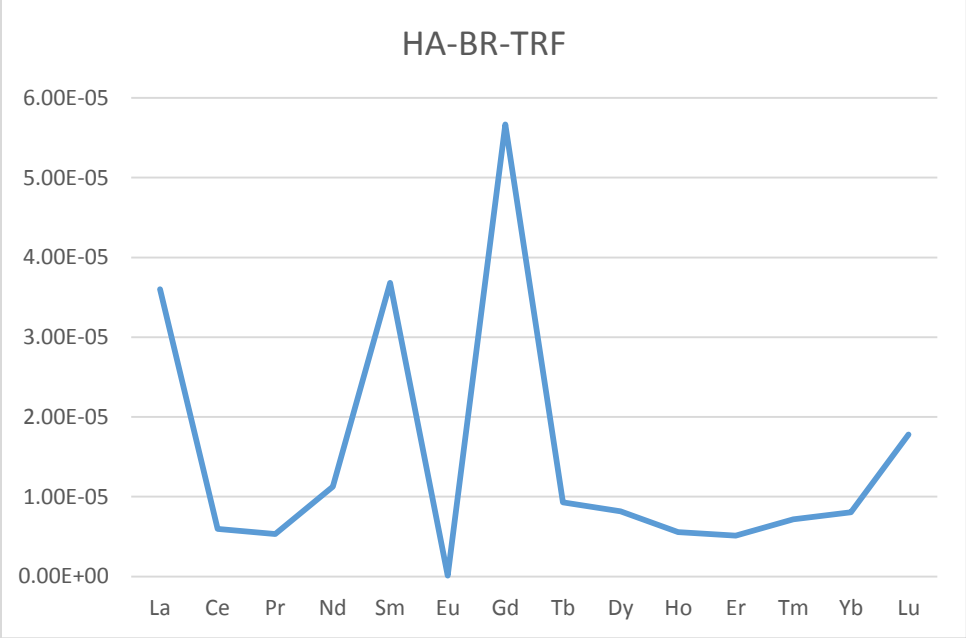

Figure 3.12 Relative distribution pattern of REE concentrations in formation water sample (HA-BR-TRF) normalized to PAAS

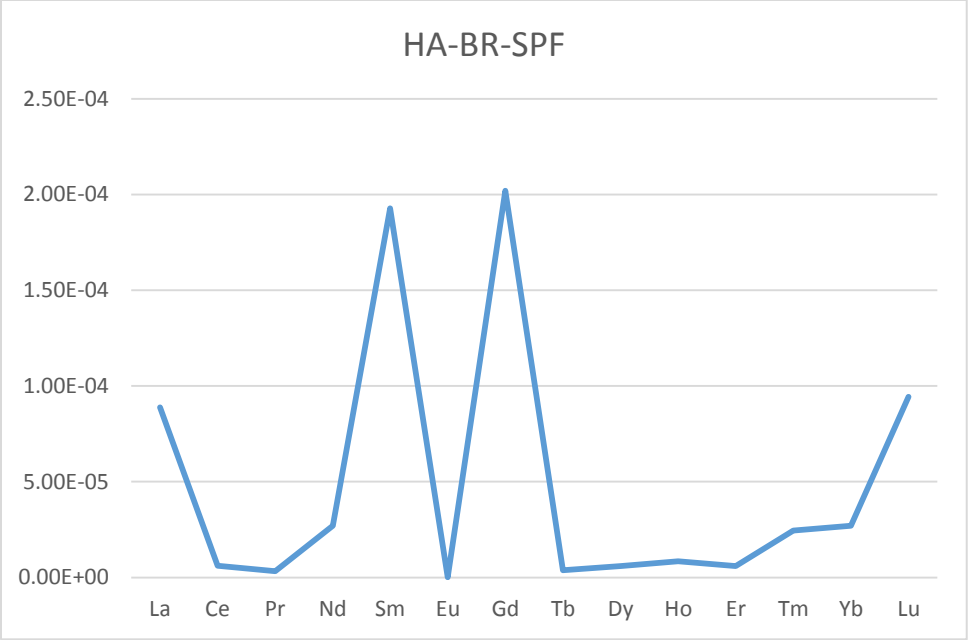

Figure 3.13 Relative distribution pattern of REE concentrations in formation water sample (HA-BR-SPF) normalized to PAAS

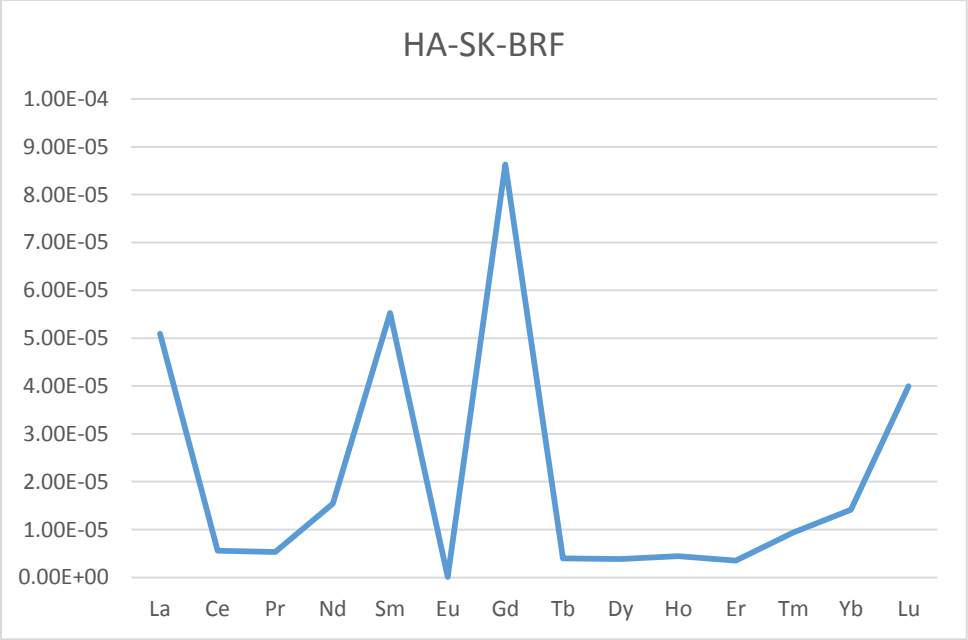

Figure 3.14 Relative distribution pattern of REE concentrations in formation water sample (HA-SK-BRF). normalized to PAAS

K/Rb Ratios of Formation Water

Formation water K/Rb ratios range from 435-599 as seen in figure 3.15. The K/Rb ratios of the formation waters have been compared to the K/Rb ratio of average silicate minerals from (Chaudhuri 2007). Similar to the crude oil samples, the formation water K/Rb ratios are above the ratio of average silicate minerals.

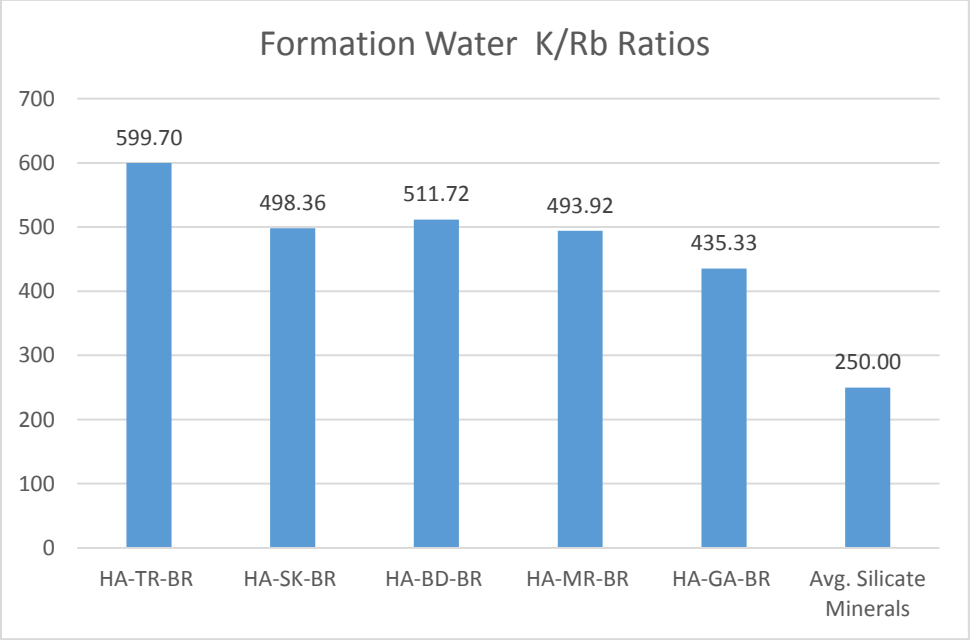

Figure 3.15 K/Rb ratios of formation water samples (HA-BD-BRF, HA-MR-BRF, HA-GA-BRF, HA-SK-BRF, HA-BR-TRF). Average of silicate minerals included for reference (Chaudhuri et al., 2007).

Seawater Evaporation Curves and Formation Water Composition

Figures 3.16-3.19 display the relative abundance of various elements in the formation water relative to sea water. These were constructed by plotting the concentrations of Ca, Mg, K, and Rb on the x-axis against the concentration of Cl on the y-axis. Curves on the chart represent

the elemental pathway in evaporating seawater. Depending where the samples plot on the chart, it can be seen whether an element relative abundance has been depleted or enriched.

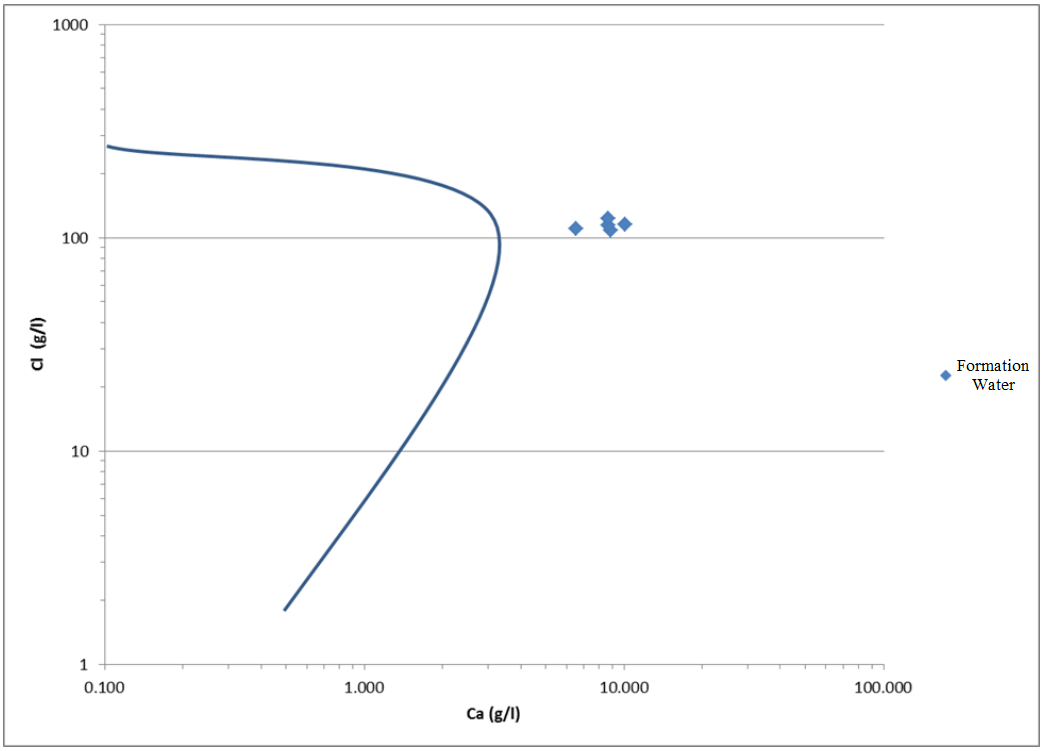

Figure 3.16 Abundance of Ca in formation water relative to seawater (solid curve), based on comparison with Cl content. The curve for evaporated seawater is based on data from Zherebtsova and Volkova (1966).

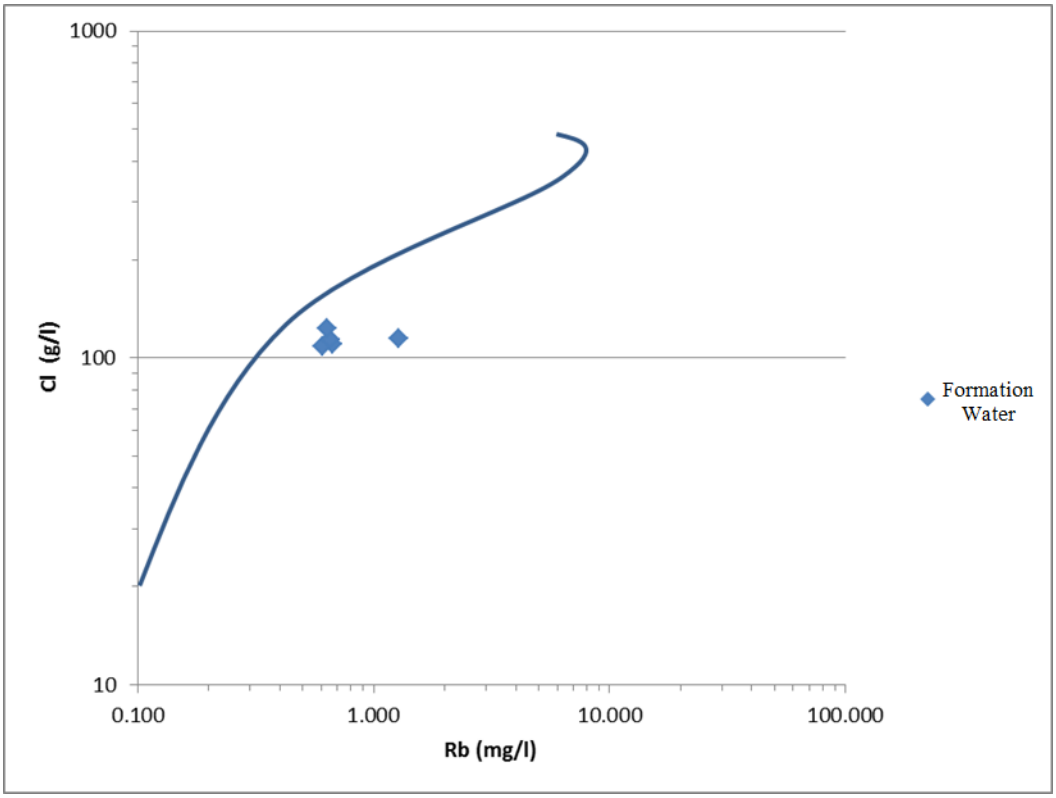

Figure 3.17 Abundance of Rb in formation water relative to seawater (solid curve), based on comparison with Cl content. The curve for evaporated seawater is based on data from Zherebtsova and Volkova (1966).

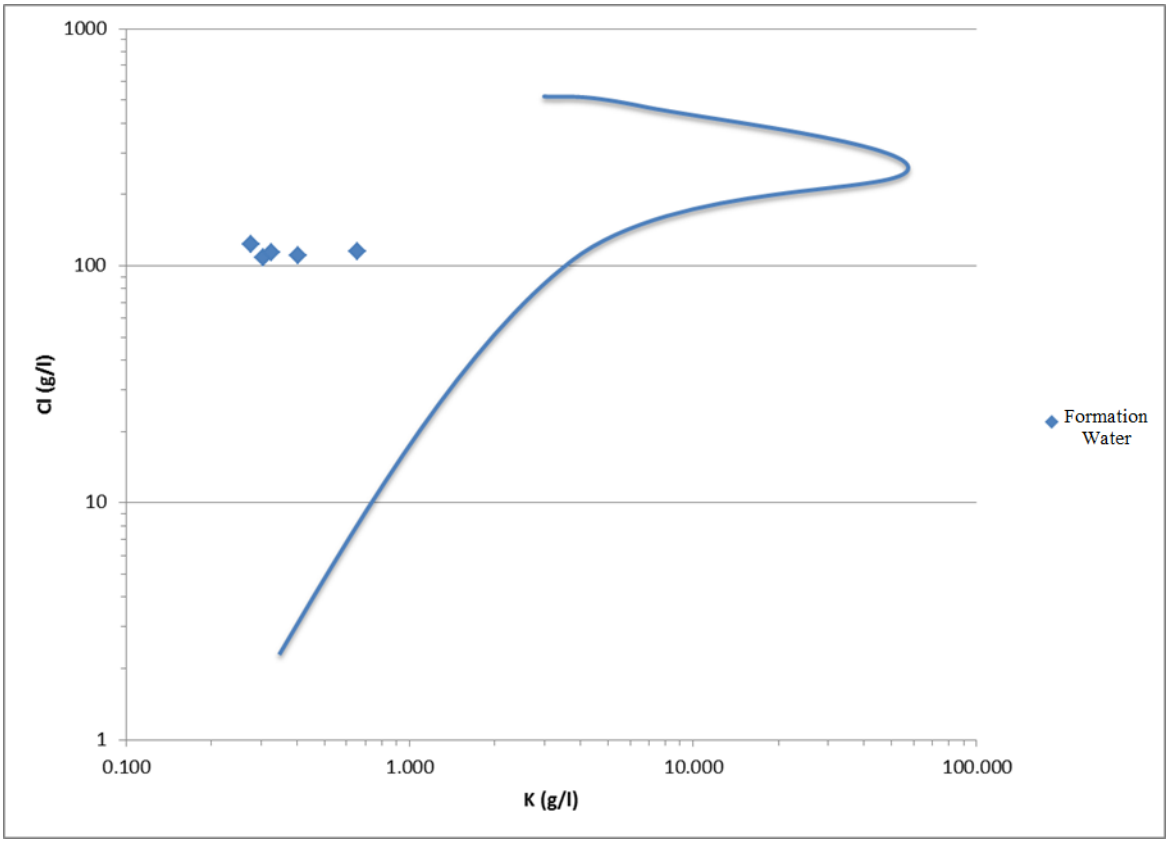

Figure 3.18 Abundance of K in formation water relative to seawater (solid curve), based on comparison with Cl content. The curve for evaporated seawater is based on data from Zherebtsova and Volkova (1966).

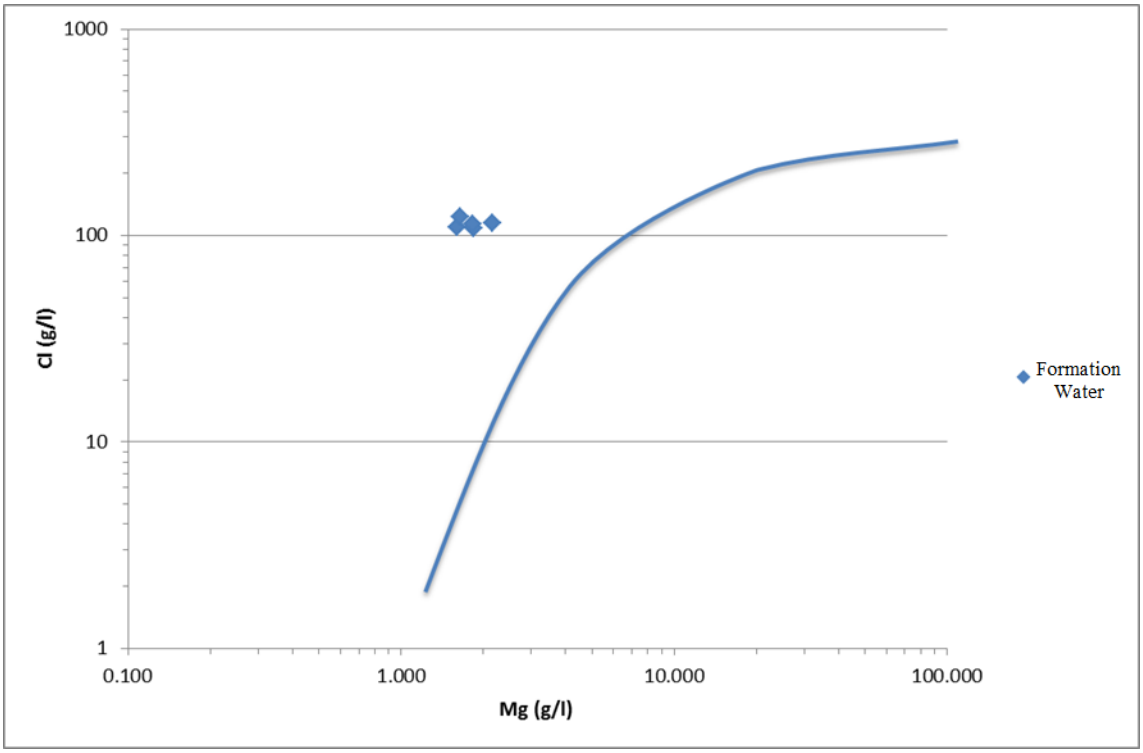

Figure 3.19 Abundance of Mg in formation water relative to seawater (solid curve), based on comparison with Cl content. The curve for evaporated seawater is based on data from Zherebtsova and Volkova (1966).

Chapter 4 - Discussion

Rare Earth Element Distribution Patterns

Rare Earth Element Distribution in Crude Oil

Crude oils are composed of roughly 2 % oxidized compounds in the form of phenols ketones, and acids Bestougeff (1967). These oxidized compounds may account for the presence of rare earth elements. In this investigation the rare earth element distribution patterns of the crude oil samples varied from one sample to another. Variations in the crude oil REE distribution patterns can be attributed to variations in the organic matter composition as shown

by Alkhammali (2015). The variations in the light rare earth elements fall into two groups with three samples showing relative enrichment and the other two samples being relatively flat. A Ce positive anomaly is present in two samples and the three other samples show a negative Ce anomaly. Each of the crude oil show relative enrichment of the middle rare earth elements. A Europium positive anomaly is present in three samples with a Eu negative anomaly present in the remaining two samples. The heavy rare earth elements in the crude oils samples contain enrichment trends in two samples with the remaining three displaying a flat trend. Anomalous behavior is present for Tm, Ho, and Yb.

Rare Earth Element Distribution in Formation Water

The rare earth element distribution patterns of the formation waters are for the most part very similar to one another. This raises the question of what is causing such a homogenous REE distribution pattern in the formation waters when compared to the distribution patterns observed in the crude oil samples. It cannot be denied that water plays an important role in the process of transformation of kerogen to bitumen to crude oil. Louis and Tissot (1967) and Lewan (1985, 1987, 1993, 1997) have recognized that two types of waters exist in hydrocarbon generating source beds. The first type is the water contained in bitumen, and the second is the water trapped in the sediment at the time of deposition. The connate water might contain variations related to the local mineral matter and organic matter. Tectonic activity over time is likely to cause micro fractures. These tiny fractures allow for primary migration of the oil, and as the oil moves out water will take its place. This process of continual mixing of formation water during hydrocarbon generation can explain the homogeneity seen in the REE distribution trends in formation water.

The crude oil, on the other hand, does not experience mixing allowing it to keep its chemical signature. Each of the six formation water samples in this investigation contains a steep light rare earth enrichment trend. The exception in the trend is Cerium, which for each of the samples a negative Ce anomaly is present. Each of the six formation water samples shows relative enrichment of the middle rare earth elements ranging from Sm to Tb. Present in all of the formation water samples is significant europium depletion relative to adjacent REE. Variation between the formation water samples is seen in the heavy rare earth elements fraction. Two trends are observed for the HREE fraction, one being a relatively flat trend absent of an anomalous behavior in four of the samples, the other being a HREE enrichment trend present in two of the formation water samples.

Middle Rare Earth Elements (MREE)

MREE Enrichment

Each of the formation water and crude oil samples show MREE enrichment trends. The enrichment found in the samples can be attributed to the influence of phosphates. Phosphate minerals are an important group of REE-bearing materials. Many phosphate phases such as apatite, monazite, and biogenic phosphates are known to be enriched in the MREE (Nagasawa, 1970; Gromet and Silver, 1983; Demartin et al., 1991; Grandjean and Albarede, 1989). Krystyniak and Paxton (2006) have concluded that phosphate nodules found in the Woodford shale are secondary in origin. This is further supported by Alkhammali 2015 analysis of the Woodford shale.

Heavy Rare Earth Elements HREE

HREE Enrichment

Two samples of formation water and two samples of crude oil exhibit an enrichment of the HREE, the remaining samples all show a flat HREE pattern. Stability constants of REE-carbonate complexes and REE-carboxylic complexes are found to increase progressively with increasing atomic number. REE-carbonate complexes or REE-carboxylate complexes or a combination of both may be the cause of HREE enrichment trends.

Specific Anomalies

Cerium Anomalies

Between the crude oil and the formation water there are nine negative anomalies for Cerium, and two positive anomalies. Source organic material variation may account for variations in the concentration of Ce in the samples. Fractionation of REEs along with its mobility in natural water is controlled partly by Mn-Oxyhydroxides. Studies (Pourret et al., 2008; Davranche et al., 2005) provide evidence that through the oxidation of Ce (III) onto the surface of MnO_2 negative anomalies of cerium are developed. In has been repeatedly reported in literature that negative Ce anomalies in terrestrial inorganic materials can be attributed to the manganese oxide precipitation effect. The formation of Mn-nodules occurs when the manganese oxide precipitates out of the seawater. These nodules found within the ocean sediment have been found to contain positive Cerium anomalies. The resulting seawater is depleted in Cerium as it sequesters into the Mn-nodules.

An additional avenue that must not be overlooked is the possibility of formation water negative Ce anomaly being derived from the kerogen. Given that the Woodford shale organic matter is primarily of marine origin, it is possible that the composition of the organic material would reflect the composition of Ce-depleted seawater. If we assume that the kerogen is

depleted in Ce, any water expelled during hydrocarbon formation should carry the same Ce negative anomaly signature. Shifting focus on the two samples with positive Ce anomalies. Pourret er al., 2008 has stated that in multiple studies Ce positive anomalies have been reported in alkaline waters. These anomalies have been suggested is the result of the stabilization of carbonato-Ce(IV)-complexes in solution that leads to an abundance of Ce (IV) compared to trivalent REEs (Moller and Bau., 1993). The idea has been present by Pourret et al., 2008 the positive Ce anomalies can be common features of alkaline, carbon-rich and aerobic waters.

Europium Anomalies

Europium negative anomalies have been found in all of the formation water samples along with two negative anomalies in the crude oil samples, leaving three crude oil samples with positive anomalies. Positive Eu anomalies have been attributed in crustal inorganic materials to crystallographic effects, especially in feldspar minerals that favor Eu^{2+} over trivalent species. In Alkhammali 2015 the drill cuttings have been found to contain feldspar and positive Eu anomalies. This can be used to interpret the pronounced negative anomalies found in the formation water samples. It is possible that the precipitation of potassium rich feldspars out of the formation water may have caused the negative anomalies in the formation water and positive anomalies in the drill cuttings. However Chaudhuri and Clauer (2007) have worked on modern plants and found positive Eu anomalies in plants relative to their growth substrates. This evidence does not support the idea of a crystallographic effect. Chaudhuri and Clauer (2007) found different Eu anomalies in different parts of the same plant. This led them to believe that plant enzyme effects play a large role in Eu anomalies in organic materials.

Holmium and Thulium Anomalies

Present in the crude oil samples are Ho and Th anomalies. The anomalies have been common with Eu and Ce in natural materials because of the difference in the oxidation states from the natural (III) oxidation state for all the REEs. Thus, Ho and Tm anomalies, varied in different degrees among the samples, and these are reflections of the growth history of the organic source material, arising potentially from enzymatic influence during the growth of the organic material.

K/Rb Ratios in Formation Water and Crude Oil

Present in all petroleum source beds is the element potassium. Potassium is found in the crystallographic structure of various mineral found in petroleum source beds. In a study by Totten and Blatt 1996 based on the average chemistry of smectite and illite they suggest that the average shale composition requires 13.4% of K-feldspar. However according to Blatt 1992 the average shale source bed only contains 5% of feldspar a potassium containing mineral, therefore secondary source of potassium is required. Organic material which is abundant in Potassium has been identified as source of Potassium in petroleum systems. As conditions change during the burial process, organic matter is transformed and the release of potassium and elements such as silicon, iron, and aluminum present in silicate minerals occurs. Chaudhuri et al. (2007) has shown that potassium together with rubidium can be a strong geochemical tracer for the source of potassium. The study shows K/Rb ratios of organic matter range from 350-10,000, much higher than the ratio in silicate minerals 50-600 with an average ratio of 250. The K/Rb ratios of formation waters for this investigation have a range of 440-692 and the crude oil ratios of 660-

1730. These ratios are indicative of the influence from the organic material as the source of potassium.

Seawater Evaporation Curves and Formation Water Composition

Organic matter must be buried rapidly otherwise the organic carbon will become susceptible to exposure to oxygen and then becoming converted to carbon dioxide. Interstitial fluids deposited at the time of burial of sediment could reasonably be of marine source. This marine water could have varied chloride content due to varied degrees of evaporation in the surrounding environments. Therefore the chemical components of the interstitial fluids may be examined by considering changes among them relative to sea water evaporation effects. In this investigation the abundances of Rb, K, Ca, and Mg relative Cl were compared to the evaporation trends of seawater from Zherebtsova and Volkova (1966). The abundances of K and Mg compared to Cl in the formation waters of this investigation are relatively depleted when compared to the data Zherebtsova and Volkova 1966. Inversely the abundances of Rb and Ca compared to Cl were found to be enriched. The formation water of this investigation has displayed both enrichment and depletion of certain cations. This raises the question of what is causing the Rb and Ca enrichment and the depletion of K and Mg.

One explanation looks into the transformation of smectite to illite, which can affect the amount of K, Rb, and Ca in our formation waters. The conversion process of smectite into illite depletes the formation water of K as illization occur. As K is substituted into smectite, the release of other cations will occur, such as Ca and Rb. However, this reaction alone cannot account for the enrichments and depletions observed in our formation water. Another process that can be considered is the dolomitization of calcite. As calcite is dolomitized the substitution of Mg for Ca occurs, which depletes the formation water Mg and enriches it with Ca this can be

observed in our formation water samples. The dolomitization of calcite along with the illitization of smectites together cannot fully account for the depletion and enrichments observed in the water. Other processes that can influence the composition of the formation water are the formation of chlorites and secondary precipitation of minerals such as K-feldspar. It is evident that one single process cannot fully account the changes in chemical composition of the formation water; instead it is a combination of process between the formation water and minerals.

Uranium/Thorium Ratios

Natural radiation occurs primarily from uranium and thorium along with their radioactive daughters' potassium and rubidium, minor radiation occurring from ^{14}C, ^{147}Sm, ^{176}Lu, and ^{187}Re. In the natural environment the important radioactive species are ^{40}K, ^{235}U, ^{238}U, and ^{232}Th, for which the ratios of U/Th have been calculated for certain rocks as seen in Gera (1975). Uranium has two oxidation states U(VI) is mobile and U(IV) is less mobile, while thorium has one oxidation state, Th(IV). In oxidizing environment Uranium has high mobility, whereas the mobility is low in reduced environments. Thorium mobility is no affected by any change in oxidation-reduction conditions of environments. Any change in U/Th ratios in sedimentary materials may therefore reflect the conditions of oxidation-reduction at the time of mineral formation.

In this study the crude oil U/Th ratios ranged from 0.45 to 1.25, whereas the formation water U/Th ratio ranged from 0.1 to 0.2. The crude oil U/Th was clearly high than the ratio of the formation water. The U/Th ratios of average shale vary between 0.3 and 0.38. The crude oil has a higher U/Th ratio than an average shale, whereas the formation water U/Th ratio is lower than the average shale. The U/Th ratio of the clay fraction of the associated shale with the crude

oil and formation water had been found to be 1.5 to 9.0 (Alkhammali, 2015). The formation water appear to be lower than either the clay fraction of the Woodford shale or the average shale. The crude oil is lower than that of the clay fraction of the Woodford Shale but higher than that of the average shale.

How could one explain the significantly lower U/Th ratios in both crude oil and formation water than the associated clay fractions, which Alkhammali analyzed? If the clay fractions consisted of components of an average shale the expected ratio should have been close to 0.3 to 0.38, a value of an average shale. The clay fraction data of Alkhammali suggests that they may contain some apatite and pyrite which are generally known for enriched amounts of uranium and thorium. Therefore the presence of these high uranium bearing minerals in the dill cutting would cause the crude oil and formation water U/Th ratios to be lower than those of the associated shales.

An explanation for crude oil having a higher U/Th ratio than formation water could be that crude oil contains more complex ligand binding sites for highly charged cations, especially having U (VI) preference over U (IV), than ligands present in formation waters. Thus a partitioning effect can be observed in which U (VI) moves favorably towards the crude oil vs the formation water. The partitioning between the crude oil and formation water cannot be the only factor for the low U/Th ratios found in the formation water

Two additional avenues in which the depletion of uranium in formation waters exist. The first involves reactions within the formation water resulting in secondary mineral production of minerals such as pyrite and apatite which are known for their accommodation of heavy elements. The second avenue that can be considered is the uptake of aqueous Uranium onto the surface of

minerals such as pyrite. The U/Th ratios between these two investigations suggest the interaction between the crude oil, formation water, and mineral matrices is indeed occurring.

Chapter 5 - Conclusions

The main significant features that emerge from this study are as followed. The specific concentration of REE and other multivalent trace element are higher in the crude oil than that in the associated formation water in source shale beds. This can be reconciled with the idea that crude oil offers more multi-dented complexes to which multivalent metals can bind than formation water (Collins, 1975). The crude oils had wide variations in REE distribution patterns; the associated formation water had a limited range of variation in the REE distribution pattern (Huc, 2013).

The complexity of the hydrocarbon generation process in a source shale bed is not fully understood. Results from oil shale retorting in early works of Engler(1913) and Frank and Goodier (1922), proved very useful to an understanding of the path of generation hydrocarbon-rich oil from kerogen. The path is essentially viewed as a two-step process. It begins with thermal decomposition of kerogen which results in the production of a polar rich bitumen fraction. Subsequent thermal decomposition of the bitumen leads to hydrocarbon-rich oil products. Louis and Tissot (1967) used this long recognized fact from oil-shale retorting studies to emphasize that petroleum formations in natural condition happen along the same two-step processes from kerogen to petroleum via bitumen products with increases in thermal stress. Lewan (1985, 1987, 1993, 1997) in a series of articles, pointing to results of hydrous pyrolysis experiments and petrographic studies, further developed this concept of petroleum formation from kerogen via bitumen formation he reported from observation of his hydrous pyrolysis that

low thermal stress between 280 to 300 degrees centigrade caused kerogen content to decrease proportionally as the polar-rich bitumen content increased until a maximum point of bitumen production reached. With further increase of thermal stress from 330 to 350 degrees centigrade, the kerogen content remained constant while the bitumen content began to decrease proportionally with increase in oil being expelled from the bitumen that impregnated the pores in the source rocks. Lewan further noted some fraction of pore water remains dissolved in the solvent polar bitumen product. A major significance of this dissolved pore water in the bitumen is that the water becomes a source of hydrogen to prevent or minimize cross-linking reactions between compounds with radical sites on carbon, and there upon promotes the development of saturate rich products, during thermal decomposition of bitumen to oil that is ultimately released into the surrounding water. Louis and Tissot (1967) earlier suggested the presences of these two distinct phases of water, one that contained with bitumen and the other into pore spaces lacking bitumen products. However, these models do not take into account all of the five elements present in petroleum source beds suggested by the Chaudhuri Totten Clauer (CTC) model.

The CTC model takes a holistic view in understanding the hydrocarbon generation process. The five regimes presented by the model are the atmosphere or gases, lithosphere or mineral matrices, hydrosphere or H2O, biosphere or organic material, and the energetics or energy produced from increasing geothermal energy or other local sources of energy such as the radioactive decay of isotopes. The first steps understanding the complex hydrocarbon generation process proposed by the CTC model, is an integration of investigations of each of the five regimes will go a long way in the understanding of the hydrocarbon generation process. This investigation, along with the work of Alkahammali (2015), Kelly (2014), McIntire (2014), and Ramirez (2013) begin to tie together each regimen of the CTC model of hydrocarbon generation.

References

Alkhammali S., 2015. Geochemical and clay mineralogical characteristic of the Woodford shale, Anadarko Basin, Oklahoma: Master's Thesis, Kansas State University,

Ball J.S., Wenger W.J., Hyden H.J., Horr C.A., and Myers A.T., 1960, Metal content of twenty four petroleums: Joournal of Chemical & Engineering Data, Vol. 5 No. 4 pp. 553-557

Bestougeff, M.A. 1967. Petroleum hydrocarbons. pp. 77-108, In B. Nagy and G. Columbo (eds.), Fundamental Aspects of Petroleum Geochemistry, Elsevier, Amsterdam

Blatt, H., 1992, Sedimentary Petrology, 2nd edition: New York, W.H., Freeman & Co., 514 p.

Bonham L.C., 1956, Geochemical investigation of crude oils: APPG Bulletin; Vol. 40 pp. 897-908

Chaudhuri S. and Clauer N., 1992. Signatures of Radiogenic Isotopes in Deep Subsurface Waters in Continents, p. 497-529. In, N. Clauer and S. Chaudhuri (Eds.) Isotope Signatures and Sedimentary Records: Springer-Verlag Berlin

Chaudhuri S., Clauer N., Semhi K., 2007. Plant decay as a major control of river dissolved potassium, A first estimate: Chemical geology, v. 243, p.178-190.

Chaudhuri et al., 2011, A study yielding the first demonstration that rare-earth elements could be a useful geochemical tracer in formation hydraulic fracturing schemes for enhanced gas and oil production: The Shale Shaker Vol. 62 No. 3 p 214-223

Collins A. G. (1975) Geochemistry of oil field waters. Elsevier

Davranche, M. O., Pourret, G., Grauau, A., Dia, M., Le Coz-Bouhnik, 2005. Adsorption of REE (III)-humate complexes onto MnO2, Experimental evidence for cerium anomaly and lanthanide tetrad effect suppression: Geochimica et Cosmochimica Acta v. 69, p. 4825-4835.

Demartin F., Pilati T., Diella V., Donzelli S. and Gramaccioli C.M., 1991, Alpine monazite: further data: Canadian Mineralogists, Vol 29, pp. 61-67

Gera F., 1975. Geochemical behavior of long-lived radioactive wastes. Oak Ridge National Laboratory Report ORNL-TM-4481. Oak Ridge Tennessee.

Grandjean P. and Albarede F., 1989, Ion probe measurement of rare earth elements in biogenic phosphates: Geochimica et Cosmochimica Acta, vol. 53, pp. 3179-3183

Gromet L.P. and Silver L.T., 1983, Rare earth element distributions among minerals in granodiorite and their petrogenic implications: Geochimica et Cosmochimica Acta, Vol 47, pp. 925-939

Hodgson G.W., 1954, Vanadium, Nickel, and iron trace metals in crude oils of Western Canada: AAPG bulletin, vol. 38, pp. 2537-2554

Huc A-Y., 2013. Geochemistry of fossil fuels. Editions Technip, Paris, France 2054 p.p.

Hunt, J.M., 1995. Petroleum Geochemistry and Geology. 2nd edition, New York: W.H. Freeman and Company.

Kidder, D.L., Eddy-Dilek, C.A., 1994. Rare-Earth Element Variation in Phosphate Nodules from Midcontinent Pennsylvanian Cyclothems: Journal of Sedimentary Research, Sedimentary Petrology and Processes, v. A64, p. 584-592.

Lewan M.D., 1985, Evaluation of petroleum generation by hydrous pyrolysis experimentation: Philosophical Transactions of the Royal Society of London, Issue 315, p. 1531

Lewan M.D., 1987, Evaluation of petroleum generation from resinites by hydrous pyrolysis: AAPG bulletin, Vol 74, pp. 394-406

Lewan M.D., 1997. Experiments on the role of water in petroleum formation: Geochimica et Cosmochimica Acta, Vol 61, pp. 3691-3723

Lewan M.D., Maynard, J.B., 1982. Factors controlling enrichment of vanadium and nickel in the bitumen of organic sedimentary rocks: Geochimica et Cosmochimica Acta, v. 46, p. 2547-2560.

Louis M.C., Tissot B.P., 1967. Influence de la temperature et da la pression sur la formation des hydrocarbures dans les arrgiles a kerogene: Seventh World Petroleum Congress Procedings 2, P. 47-60.

McIntire M.C., 2014. Rare earth elements (REE) in crude oil in the Lansing-Kansas City formations in central Kansas: potential indications about their sources, locally derived or long-distance derived: Master's Thesis, Kansas State University,

Moller, P. and Bau, M., 1993, Rare-earth patterns with positive cerium anomaly in alkaline waters from Lake Van, Turkey: Earth Planet. Sci Lett, v. 117, p. 671-676.

Nagasawa H., 1970, Rare earth concentration in Zircons and apatites and their host dacites and granites: Earth and Planetary Science Letters, Vol. 9, pp. 359-364

Pourmand A., Dauphas, N., Ireland, T.J., 2012. A novel extraction chromatography and MC-ICP-MS technique for rapid analysis of REE, Sc and Y, Revising CI-chondrite and Post-Archean Australian Shale (PAAS) abundances: Chemical Geology v. 291, p. 38-54.

Pourret et al., 2008 New insights into cerium anomalies in organic-rich alkaline water: Chem. Geol., 251, pp. 120-127

Puckette J., 2013. Characteristics of Devonian-Mississippian strata in the Southern midcontinent: AAPG Woodford Shale Forum, April, 2013, Oklahoma City, OK

Ramirez D., 2013. Rare Earth Elements (REE) as Geochemical Clues to Reconstruct Hydrocarbon Generation History: Master's Thesis, Kansas State University,

Rollinson, H.R., 1993. Using Geochemical Data, Evaluation, Presentation, Interpretation. 1st edition, England: Pearson Education Limited.

Topp, N. E., 1965. The Chemistry of Rare Earth Elements: Amsterdam, Elsevier Publishing Company, 345 p.

Totten, M. W., Blatt H., 1996. Sources of silica from the illite to muscovite transformation during late-stage diagenesis of shales, Siliciclastic diagenesis and fluid flow, Concepts and Applications: Society of Economic Paleontologists and Mineralogists, Special Publication No. 55, p. 85-92.

Yen T.F., 1975, Chemical aspects of metals in native petroleum: The Role of Trace Metals in Petroleum, Ann Arbor Science Publishers 1, pp. 1-32

Witherspoon P.A., Nagashima K., 1957, Use of Trace Metals to Identify Illinois Crude Oils: Illinois State Geological Survey, 16 p.

Zherebtsova I.K. and Volkova N.N. (1966) Experimental study of behavior of trace elements in the process of natural solar evaporation of Black sea water and Sasyk-sivash brine. Geochem. Intl. 3, 656-670

Appendix A - Rare Earth Distribution Trends

Formation Water Samples

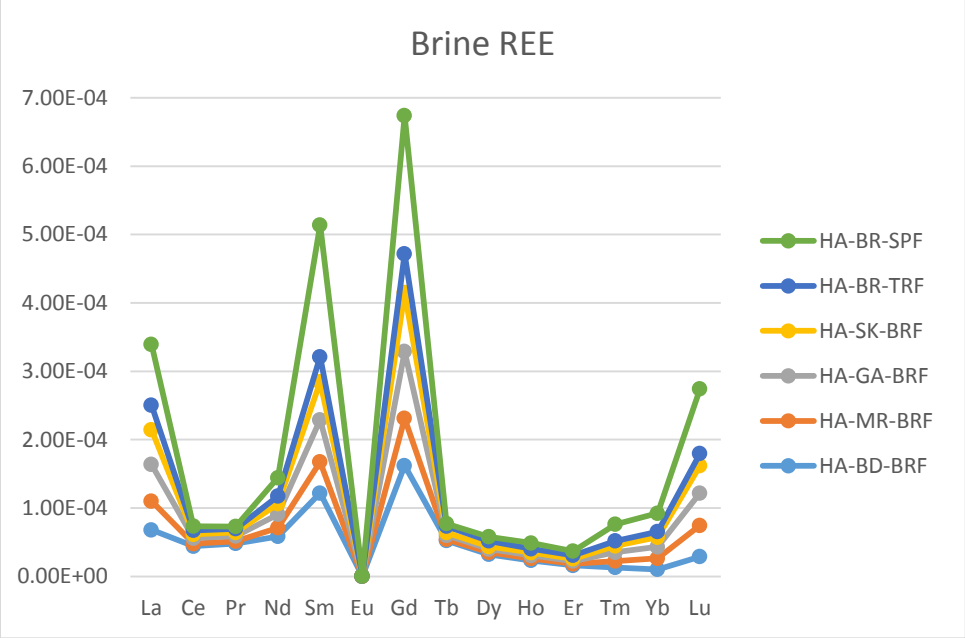

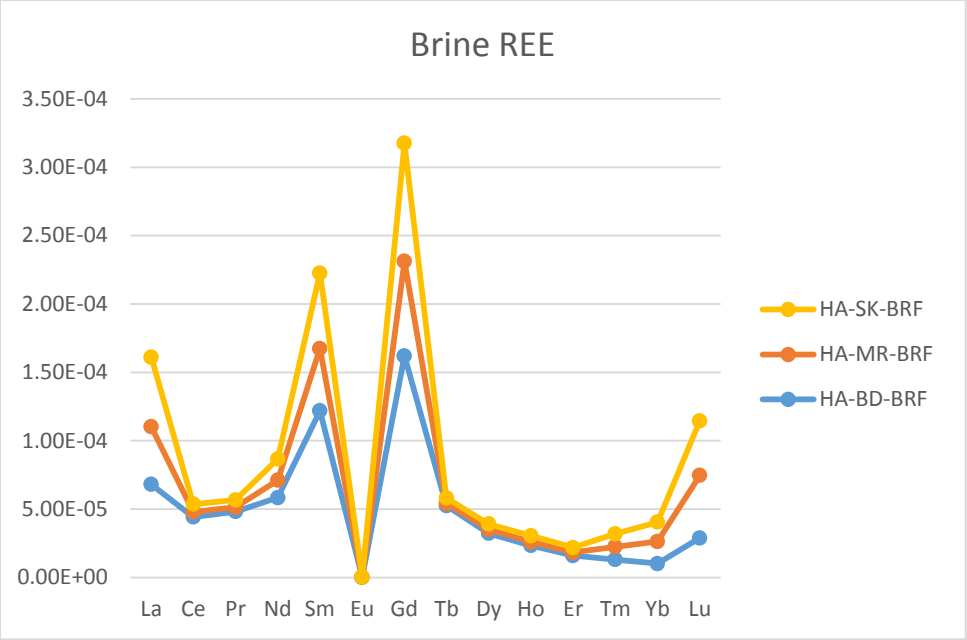
Brine REE
3.50E-04
3.00E-04
2.50E-04
2.00E-04
1.50E-04
1.00E-04
5.00E-05
0.00E+00
La Ce Pr Nd Sm Eu Gd Tb Dy Ho Er Tm Yb Lu
HA-SK-BRF
HA-MR-BRF
HA-BD-BRF

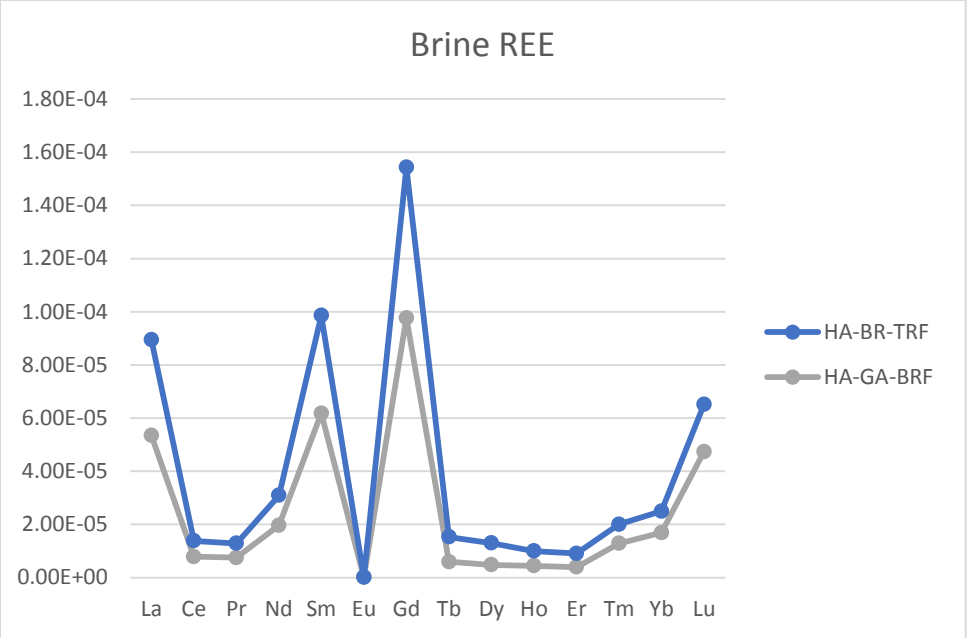
Brine REE
1.80E-04
1.60E-04
1.40E-04
1.20E-04
1.00E-04
8.00E-05
6.00E-05
4.00E-05
2.00E-05
0.00E+00
La Ce Pr Nd Sm Eu Gd Tb Dy Ho Er Tm Yb Lu
HA-BR-TRF
HA-GA-BRF

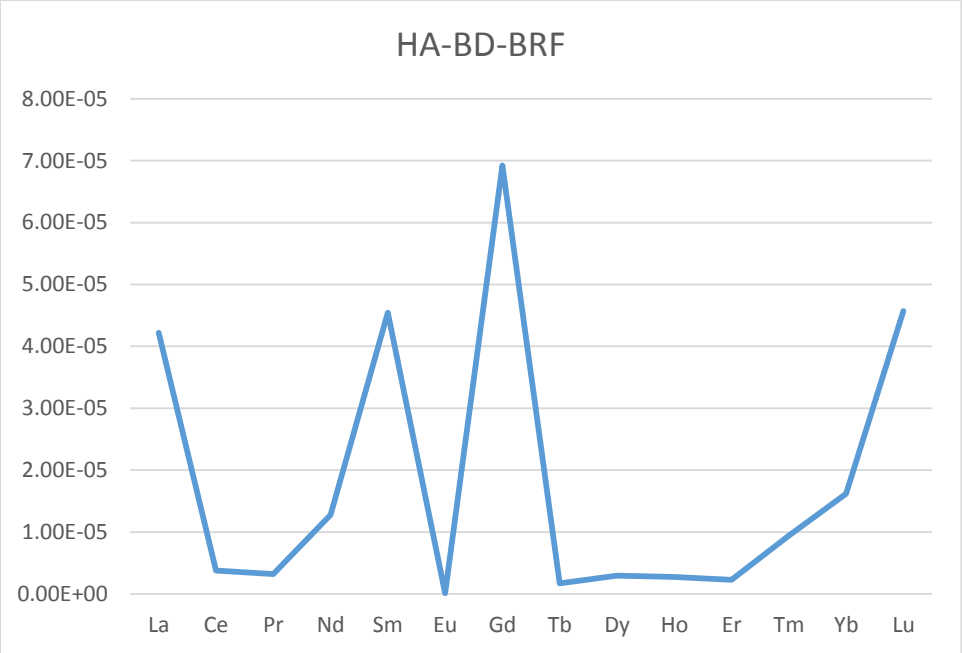
HA-BD-BRF
8.00E-05
7.00E-05
6.00E-05
5.00E-05
4.00E-05
3.00E-05
2.00E-05
1.00E-05
0.00E+00
La
Ce
Pr
Nd
Sm
Eu
Gd
Tb
Dy
Ho
Er
Tm
Yb
Lu

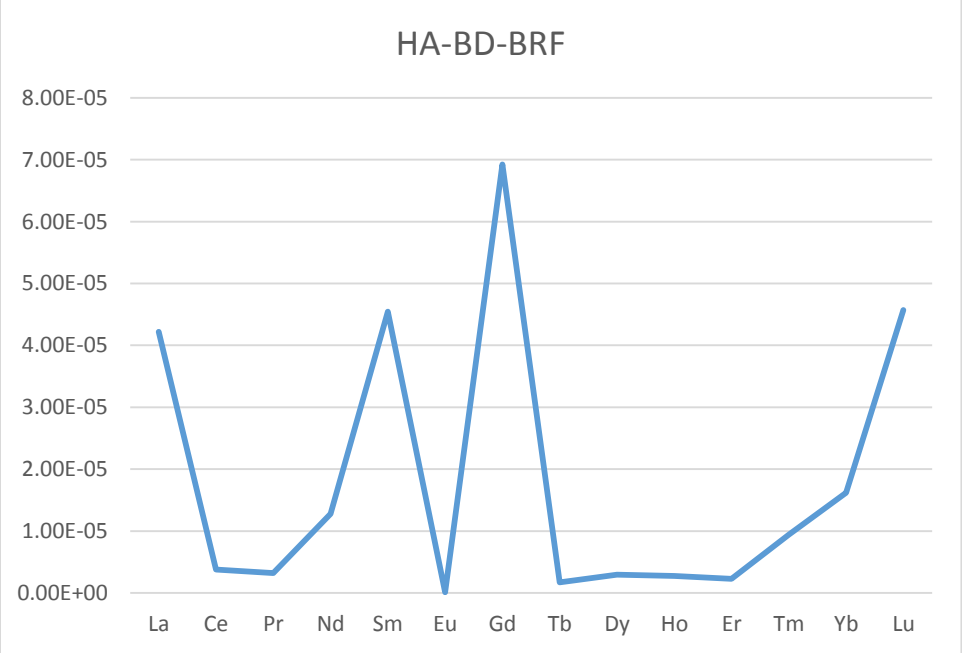
HA-BD-BRF
8.00E-05
7.00E-05
6.00E-05
5.00E-05
4.00E-05
3.00E-05
2.00E-05
1.00E-05
0.00E+00
La
Ce
Pr
Nd
Sm
Eu
Gd
Tb
Dy
Ho
Er
Tm
Yb
Lu

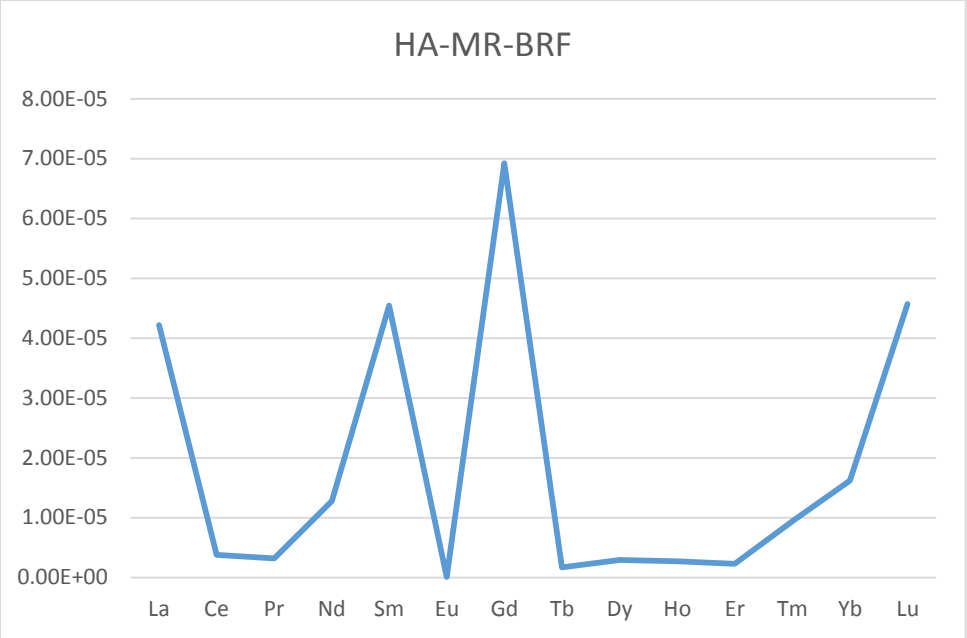
HA-MR-BRF
8.00E-05
7.00E-05
6.00E-05
5.00E-05
4.00E-05
3.00E-05
2.00E-05
1.00E-05
0.00E+00
La Ce Pr Nd Sm Eu Gd Tb Dy Ho Er Tm Yb Lu

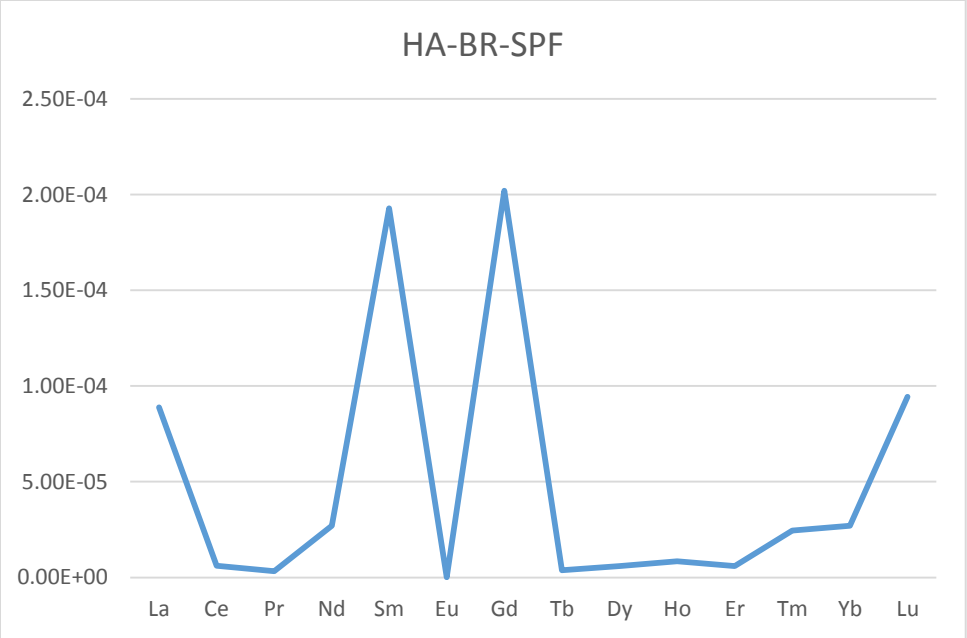
HA-BR-SPF
2.50E-04
2.00E-04
1.50E-04
1.00E-04
5.00E-05
0.00E+00
La Ce Pr Nd Sm Eu Gd Tb Dy Ho Er Tm Yb Lu

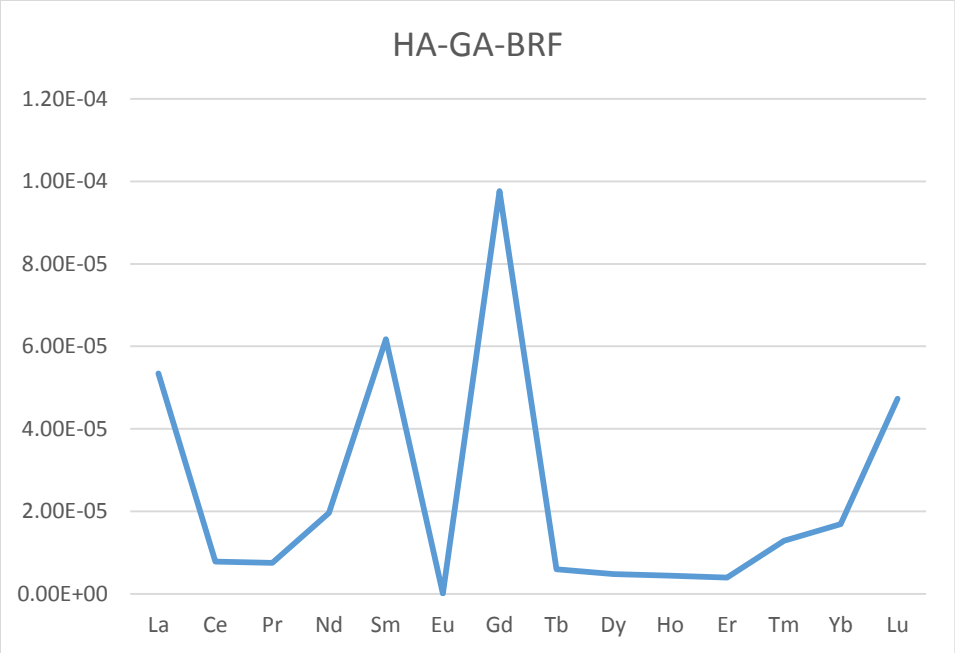
HA-GA-BRF
1.20E-04
1.00E-04
8.00E-05
6.00E-05
4.00E-05
2.00E-05
0.00E+00
La
Ce
Pr
Nd
Sm
Eu
Gd
Tb
Dy
Ho
Er
Tm
Yb
Lu

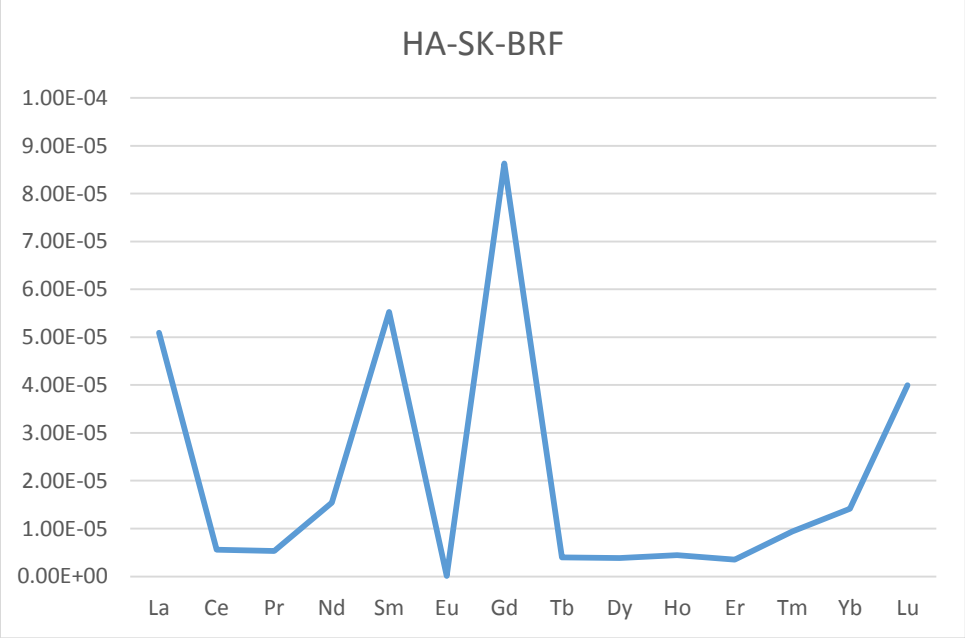
HA-SK-BRF
1.00E-04
9.00E-05
8.00E-05
7.00E-05
6.00E-05
5.00E-05
4.00E-05
3.00E-05
2.00E-05
1.00E-05
0.00E+00
La
Ce
Pr
Nd
Sm
Eu
Gd
Tb
Dy
Ho
Er
Tm
Yb
Lu

élément	HA-BD-BRF	HA-MR-BRF	HA-GA-BRF	HA-SK-BRF	HA-BR-TRF	HA-BR-SPF
La	6.806282722513090E-05	4.217277486910990E-05	5.345549738219900E-05	5.091623036649210E-05	3.599476439790580E-05	8.882198952879580E-05
Ce	4.415829145728640E-05	3.768844221105530E-06	7.839195979899500E-06	5.603015075376880E-06	5.979899497487440E-06	6.118090452261310E-06
Pr	4.817667044167610E-05	3.204983012457530E-06	7.531143827859570E-06	5.311438278595700E-06	5.334088335220840E-06	3.352208380520950E-06
Nd	5.840707964601770E-05	1.274926253687320E-05	1.965191740412980E-05	1.538643067846610E-05	1.125958702064900E-05	2.694985250737460E-05
Sm	1.219279279279280E-04	4.545945945945950E-05	6.176576576576580E-05	5.526126126126130E-05	3.681081081081080E-05	1.927927927927930E-04
Eu	9.259259259259260E-08	9.259259259259260E-08	9.259259259259260E-08	9.259259259259260E-08	9.259259259259260E-08	9.259259259259260E-08
Gd	1.620171673819740E-04	6.922746781115880E-05	9.763948497854080E-05	8.633047210300430E-05	5.667381974248930E-05	2.020600858369100E-04
Tb	5.245478036175710E-05	1.679586563307490E-06	5.943152454780360E-06	4.005167958656330E-06	9.302325581395350E-06	3.746770025839790E-06
Dy	3.226495726495730E-05	2.927350427350430E-06	4.786324786324790E-06	3.824786324786320E-06	8.183760683760680E-06	6.025641025641030E-06
Ho	2.330978809283550E-05	2.724520686175580E-06	4.439959636730580E-06	4.439959636730580E-06	5.549949545913220E-06	8.375378405650860E-06
Er	1.603508771929820E-05	2.280701754385960E-06	3.964912280701750E-06	3.508771929824560E-06	5.122807017543860E-06	5.894736842105260E-06
Tm	1.308641975308640E-05	9.382716049382710E-06	1.283950617283950E-05	9.382716049382710E-06	7.160493827160490E-06	2.444444444444440E-05
Yb	1.017730496453900E-05	1.617021276595740E-05	1.687943262411350E-05	1.414893617021280E-05	8.049645390070920E-06	2.695035460992910E-05
Lu	2.886836027713630E-05	4.572748267898380E-05	4.734411085450350E-05	3.995381062355660E-05	1.778290993071590E-05	9.445727482678980E-05

Crude oil samples

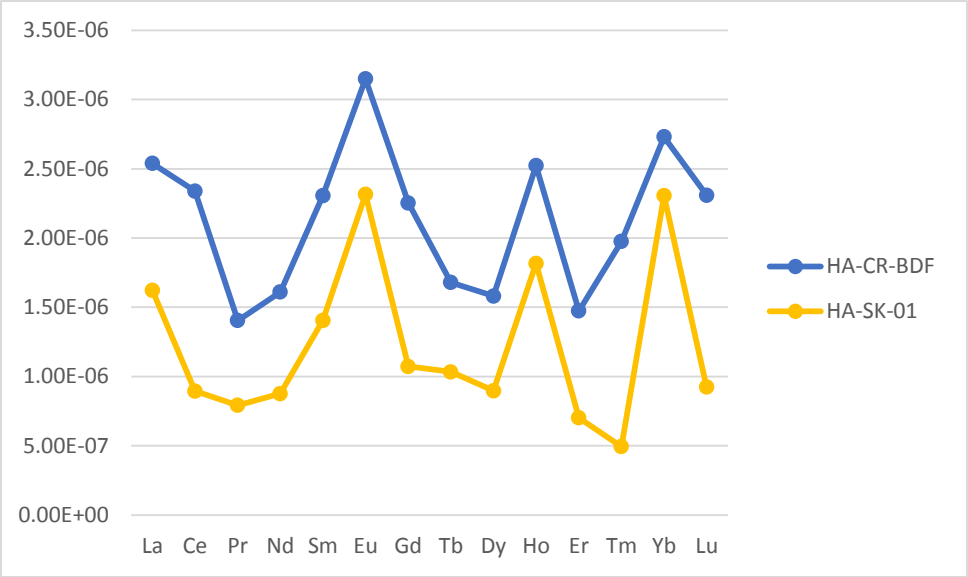

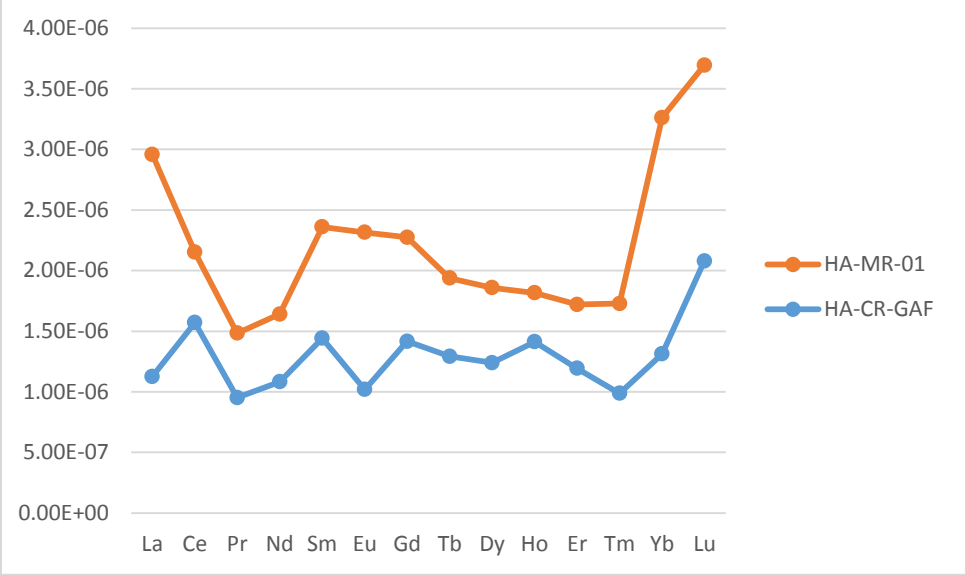

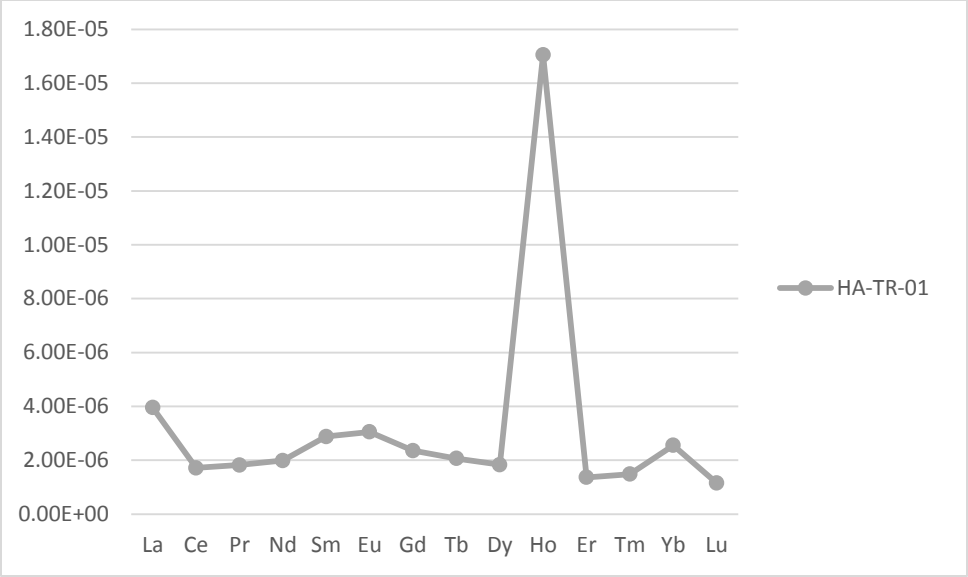

élément	HA-CR-BDF	HA-SK-01	HA-TR-01	HA-MR-01	HA-CR-GAF
La	9.1623E-07	1.62304E-06	3.95288E-06	1.83246E-06	1.12565E-06
Ce	1.44472E-06	8.94472E-07	1.71859E-06	5.81658E-07	1.57035E-06
Pr	6.11552E-07	7.92752E-07	1.82333E-06	5.32276E-07	9.51302E-07
Nd	7.34513E-07	8.76106E-07	1.99115E-06	5.57522E-07	1.0826E-06
Sm	9.00901E-07	1.40541E-06	2.88288E-06	9.18919E-07	1.44144E-06
Eu	8.33333E-07	2.31481E-06	3.05556E-06	1.2963E-06	1.01852E-06
Gd	1.18026E-06	1.07296E-06	2.36052E-06	8.58369E-07	1.41631E-06
Tb	6.45995E-07	1.03359E-06	2.06718E-06	6.45995E-07	1.29199E-06
Dy	6.83761E-07	8.97436E-07	1.83761E-06	6.19658E-07	1.23932E-06
Ho	7.06357E-07	1.81635E-06	1.70535E-05	4.03633E-07	1.41271E-06
Er	7.7193E-07	7.01754E-07	1.36842E-06	5.26316E-07	1.19298E-06
Tm	1.48148E-06	4.93827E-07	1.48148E-06	7.40741E-07	9.87654E-07
Yb	4.25532E-07	2.30496E-06	2.55319E-06	1.95035E-06	1.31206E-06
Lu	1.38568E-06	9.23788E-07	1.15473E-06	1.61663E-06	2.07852E-06

	Eu/Eu*	Ce/Ce*
HA-CR-BDF	0.80083604	1.89126946
HA-SK-01	1.86801634	0.74052204
HA-TR-01	1.16548681	0.59505912
HA-MR-01	1.4587352	0.49194331
HA-CR-GAF	0.71281138	1.51216601

Appendix B - Calculated Data

Seawater Evaportaion Curves and Formation Water Composition

	Cl-	Ca	K	Mg	Rb
HA-TR-BR	110.041	6.52	0.403	1.6	0.672
HA-SK-BR	108.59	8.86	0.304	1.84	0.61
HA-BD-BR	114.997	10.1	0.655	2.16	1.28
HA-MR-BR	114.11	8.68	0.325	1.83	0.658
HA-GA-BR	123.36	8.7	0.276	1.65	0.634